electronics

MDPI

Article

Multi-Method Diagnosis of CT Images for Rapid Detection of Intracranial Hemorrhages Based on Deep and Hybrid Learning

Badiea Abdulkarem Mohammed [1,2,*,†], Ebrahim Mohammed Senan [3,†], Zeyad Ghaleb Al-Mekhlafi [4,†], Taha H. Rassem [5,†], Nasrin M. Makbol [6,†], Adwan Alownie Alanazi [4,†], Tariq S. Almurayziq [4,†], Fuad A. Ghaleb [7] and Amer A. Sallam [8]

1 Department of Computer Engineering, College of Computer Science and Engineering, University of Ha'il, Ha'il 81481, Saudi Arabia
2 College of Computer Science and Engineering, Hodeidah University, Hodiedah 967, Yemen
3 Department of Computer Science & Information Technology, Dr. Babasaheb Ambedkar Marathwada University, Aurangabad 431004, India
4 Department of Information and Computer Science, College of Computer Science and Engineering, University of Ha'il, Ha'il 81481, Saudi Arabia
5 Faculty of Science and Technology, Bournemouth University, Poole BH12 5BB, UK
6 Centre for Software Development & Integrated Computing (Software Centre), Universiti Malaysia Pahang, Gambang 26300, Malaysia
7 School of Computing, Faculty of Engineering, Universiti Teknologi Malaysia, Johor Bahru 81310, Malaysia
8 Engineering and Information Technology College, Taiz University, Taiz 6803, Yemen
* Correspondence: b.alshaibani@uoh.edu.sa
† These authors contributed equally to this work.

Abstract: Intracranial hemorrhaging is considered a type of disease that affects the brain and is very dangerous, with high-mortality cases if there is no rapid diagnosis and prompt treatment. CT images are one of the most important methods of diagnosing intracranial hemorrhages. CT images contain huge amounts of information, requiring a lot of experience and taking a long time for proper analysis and diagnosis. Thus, artificial intelligence techniques provide an automatic mechanism for evaluating CT images to make a diagnosis with high accuracy and help radiologists make their diagnostic decisions. In this study, CT images for rapid detection of intracranial hemorrhages are diagnosed by three proposed systems with various methodologies and materials, where each system contains more than one network. The first system is proposed by three pretrained deep learning models, which are GoogLeNet, ResNet-50 and AlexNet. The second proposed system using a hybrid technology consists of two parts: the first part is the GoogLeNet, ResNet-50 and AlexNet models for extracting feature maps, while the second part is the SVM algorithm for classifying feature maps. The third proposed system uses artificial neural networks (ANNs) based on the features of the GoogLeNet, ResNet-50 and AlexNet models, whose dimensions are reduced by a principal component analysis (PCA) algorithm, and then the low-dimensional features are combined with the features of the GLCM and LBP algorithms. All the proposed systems achieved promising results in the diagnosis of CT images for the rapid detection of intracranial hemorrhages. The ANN network based on fusion of the deep feature of AlexNet with the features of GLCM and LBP reached an accuracy of 99.3%, precision of 99.36%, sensitivity of 99.5%, specificity of 99.57% and AUC of 99.84%.

Keywords: CNN models; hybrid method; ANN; SVM; hemorrhage diseases; LBP; GLCM; PCA

Citation: Mohammed, B.A.; Senan, E.M.; Al-Mekhlafi, Z.G.; Rassem, T.H.; Makbol, N.M.; Alanazi, A.A.; Almurayziq, T.S.; Ghaleb, F.A.; Sallam, A.A. Multi-Method Diagnosis of CT Images for Rapid Detection of Intracranial Hemorrhages Based on Deep and Hybrid Learning. *Electronics* **2022**, *11*, 2460. https://doi.org/10.3390/electronics11152460

Received: 10 June 2022
Accepted: 4 August 2022
Published: 7 August 2022

1. Introduction

An intracranial hemorrhage (ICH) involves bleeding that occurs in an intracranial vault [1]. This disease represents a high-risk health problem that requires prompt diagnosis and treatment. ICHs account for about 10–30% of strokes, but it is the most dangerous type of stroke, accounting for 35–52% of deaths compared with other strokes. They are also the fifth leading cause of death in the United States of America [2]. The most critical factors of

infection of an ICH are high blood pressure, weak blood vessels, external trauma to the skull, drug abuse and leakage into the veins associated with the ICH. The major types of ICHs are epidural hemorrhages, subdural hemorrhages, subarachnoid hemorrhages and intraventricular and intraparenchymal hemorrhages [3]. According to the American Stroke Association, early diagnosis and prompt and timely treatment of the patient is necessary, because these cases can kill the patient after they occur [4]. For medical treatment of disorders that cause cerebral hemorrhaging, determining the type and location of bleeding is essential for the patient's treatment. Therefore, to examine disorders, doctors rely on many imaging techniques of the brain's internal structures, such as angiography (CTA), magnetic resonance imaging and computer tomography (CT) of the head. CT is considered one of the best medical techniques used to diagnose cerebral hemorrhages because of its advantages, such as its high sensitivity to blood and the short scanning time, showing the bleeding area with a high density [5]. Thus, CT provides accurate and reliable information that the radiologist can diagnose an ICH with, as well as the amount of bleeding and its location in the patient. Strokes caused by reduced blood flow to the brain have clinical characteristics similar to ICHs, and therefore treatment differs significantly between strokes and cerebral hemorrhages. Therefore, prompt and accurate diagnosis by doctors and radiologists is critical to dealing with a cerebral hemorrhage and its location [6], though there is a lack of highly experienced radiologists, especially in developing countries. Additionally, analyzing all the data in CT images requires highly experienced specialists, as well as great effort and a lot of time. Due to the increase of big data in CT, patients have the risk of misdiagnosis. Although highly experienced radiologists are limited in analyzing massive CT image data [7], it is not easy to obtain correct diagnostic results in a short time [8]. Thus, artificial intelligence techniques helped experts, radiologists and patients with their high speeds to analyze all CT image data with high accuracy and determine the type and location of a cerebral hemorrhage. Artificial intelligence algorithms have achieved effective performance and high speeds in recent years. Deep learning models have shown superior generalizability for solving complex medical problems such as analyzing and forming diagnoses from medical images [9], discovering diseases [10] and detecting internal organs [11]. CNN models are the most efficient and effective because they have many convolutional layers to extract more complex deep feature maps that cannot be detected manually. Several CNN models have been developed, such as GoogLeNet, AlexNet, ResNet-xx, MobileNet and VGG [12]. All of these models were extensively trained on a dataset called ImageNet, which contains more than a million images for classifying into more than a thousand classes [13]. However, ImageNet does not contain many medical images, though these models can be used with the transfer learning method. The transfer learning method builds on the experience gained by CNN models to perform new tasks of classifying medical datasets [14–16]. In this study, several proposed systems, materials and methods are applied to diagnose the CT images of a hemorrhage dataset. The first proposed system is pretrained CNN models to perform new tasks on a new dataset. The second system uses hybrid techniques between CNN models and machine learning algorithms. The third system extracts features in a hybrid method between CNN models and GLCM and LBP algorithms and then feeds them to ANN neural networks to classify them. This study contains the following major contributions:

- Removing all noise and artifacts and showing the hemorrhage's edges using overlapping filters;
- Adjusting the training options for CNN models for the best performance;
- Applying hybrid technology consisting of two blocks: the first block being deep learning models for feature extraction and the second block being an SVM algorithm for classifying the extracted features;
- Reducing the dimensions of the features extracted from the deep learning models using the PCA algorithm and combining them with the features of the GLCM and LBP algorithms;
- Developing automated systems to assist radiologists in supporting their decisions for saving patients' lives.

The remainder of the paper is organized as follows. Section 2 reviews the previous relevant studies. Section 3 describes the methodological mechanism of the proposed methods for analyzing and evaluating CT images for early detection of the hemorrhage disease. Section 4 summarizes the experimental results of each proposed method. Section 5 presents a discussion of the proposed methods and compares the diagnostic results of all the proposed methods. Section 6 concludes the study.

2. Related Work

This section presents a set of previous studies related to the diagnosis of hemorrhage dataset. This study was distinguished by the diversity of methods and methodologies for analyzing the dataset and reaching superior results in indicating which image contained an ICH.

Awwal et al. presented an AlexNet model and AlexNet-SVM network method for locating cerebral hemorrhages through CT for the hemorrhage dataset. The dataset was classified by a pretrained AlexNet model built from scratch in addition to the AlexNet-SVM hybrid method. The experiments proved the superiority of AlexNet-SVM over the rest of the models [17]. Anas et al. proposed a CNN model for diagnosing 200 samples from the dataset with secondary data for the classification of hemorrhages. This method achieved an accuracy of 93.14% [18]. Sofia et al. proposed a CNN and supervised machine learning to diagnose the dataset as bleeding or healthy. Images were processed for noise removal and edge extraction by a watershed and feature extraction, and they were classified using the SVM and CNN models [19]. Xiaohong et al. proposed a method based on deep learning to classify and segment the cerebral hemorrhage zone. To effectively segment the cerebral hemorrhage area requires sufficient information, and because the large parameters of the model do not make the model reach the optimum level, Bayesian-based deep learning and hybrid models were thus applied to classify the bleeding site effectively [20]. Romany et al. proposed a deep learning model for diagnosing ICHs. The model first includes image preprocessing and segmentation by an elephant herd optimization (EHO) algorithm and then applies the Inception v4 model to extract deep feature maps. The deep feature maps were classified by the multilayer perceptron (MLP) [21]. Jiajie et al. proposed two neural networks, EfficientNet-B3 and SE-ResNeXt50, to classify intracerebral hemorrhages based on feature extraction. The models performed better than the experts for the classification of cerebral hemorrhages, achieving a score of 0.0548 during the testing phase [22]. Ruijuan et al. discuss a method for discovering brain engineering data based on a three-dimensional brain model consisting of four layers of brain structure reconstruction. Then, they applied four CNN models to solve the problem of restructuring the brain, which achieved good results [23]. Lu et al. proposed a U-net-based CNN methodology to detect the locations and strokes of bleeding in CT images. The methodology enhances the difference between the normal brain tissue and the bleeding area by comparing different CNN models through changing layers and expansion rates, which increases the acquisition of the lesion features' information [24]. Tomasz et al. proposed the ResNet-50 model to determine bleeding quickly and efficiently. The system achieved an accuracy of 93.3% and recall of 76% [25]. Luis et al. presented an automated approach based on deep learning EfficientDet to classify CT images for classification as either a cerebral hemorrhage or healthy, which achieved an accuracy of 92.7%. It also provides a visual interpretation by the Grad-CAM method [26]. Ali et al. proposed a deep learning methodology with deep supervision (CNN-DS) to segment the lesion area and measure the volume of bleeding within the brain. The data were trained and tested by the CNN-DS model. The methodology achieved a dice coefficient of 0.84 ± 0.06 and recall of 83% [27]. Young et al. proposed an artificial neural network (ANN) algorithm to detect cerebral hemorrhages and determine their type. For the classification of cerebral hemorrhages, the algorithm achieved a sensitivity of 78% and an AUC of 85.9%. It reached a sensitivity of 82.5% and an AUC of 90.3% for the localization of cerebral hemorrhages [28]. Anupama et al. proposed a synergic deep learning model using the GrabCut segmentation method called GC-SDL. Images were enhanced by a Gabor filter

and bleeding area segmentation with GrabCut to separate the bleeding areas from the healthy areas. Synergic deep learning extracted deep feature maps and categorized them with softmax, achieving an accuracy and sensitivity of 95.73% and 94.01%, respectively [29]. Junghwan et al. introduced a method of two sequential CNNs and dual fully convolutional networks (FCNs) to detect a cerebral haemorrhage type and location. Binary classification and bleeding area extraction were also applied, which performed better than the CNN and FCNs. It achieved a hash of 80.19%, compared with the accuracy of 76.75% achieved by the FCNs [30].

3. Methods and Materials

This section reviews the various methodologies and methods for evaluating CT images for early hemorrhage disease detection. The first step in this work was to optimize all images to remove artifacts and reveal the edges of the hemorrhage area. Three proposed systems classified the dataset. First, the dataset was classified using deep learning through the GoogLeNet, ResNet-50 and AlexNet models. Second, the dataset was classified by a hybrid technique between the deep learning models and the SVM algorithm. Third, the dataset was classified by an ANN based on the hybrid features between the deep learning models and the GLCM and LPB algorithms as shown in Figure 1.

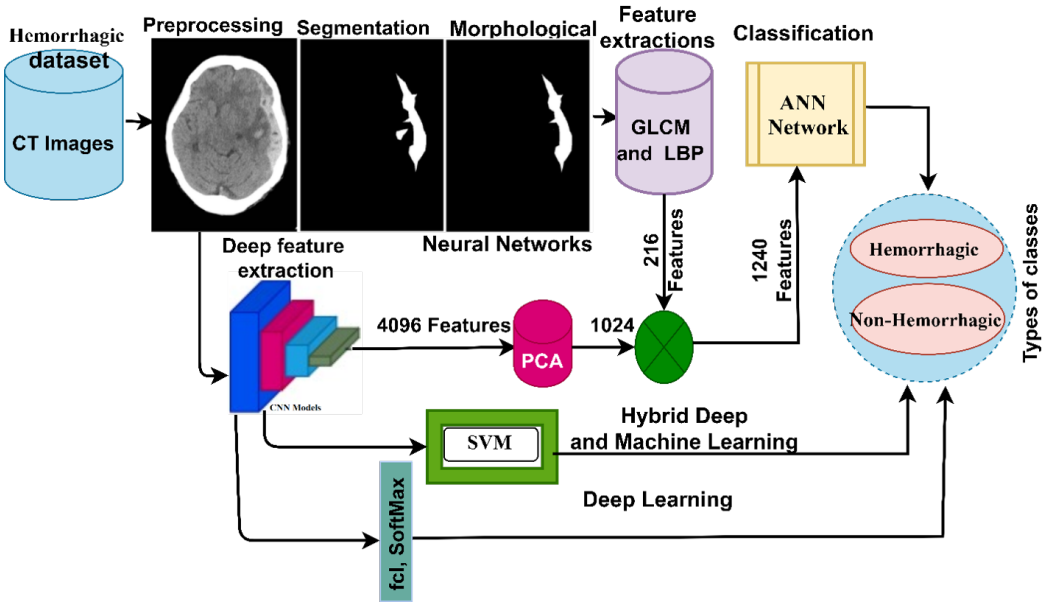

Figure 1. Proposed methodology for diagnosing CT images for early detection of hemorrhage disease.

3.1. Description of the Dataset

This study evaluated all the proposed systems on the CT dataset for hemorrhages collected from the Near East Hospital in Cyprus [31]. The list of risk factors that leads to a hemorrhage is as follows:

1. Patients with diabetes in their clinical histories, plasma glucose of 200 mg/dL, fasting ≥126 mg/dL or glycated haemoglobin of 6.5%;
2. The ratio of cholesterol and lipoprotein is 100 mg, and the triglycerides are at 150 mg/dL;
3. Arterial blood pressure is a systolic 140 mm Hg or diastolic 90 mm Hg;
4. Patients with cardiovascular diseases and atherosclerosis.

The dataset consists of 7032 CT brain images obtained from 18 patients with cerebral hemorrhages and 27 people without cerebral hemorrhages. Everyone has many CT images of their brains. The dataset is divided into two categories, where 2689 hemorrhagic and 4343 healthy non-hemorrhagic images were all acquired in the medical digital imaging format with a resolution of 512 × 512 pixels. Figure 2 shows samples from the dataset that

were randomly selected for the hemorrhagic and non-hemorrhagic classes (https://www.kaggle.com/abdulkader90/brain-ct-hemorrhage-dataset (accessed on 1 May 2022)).

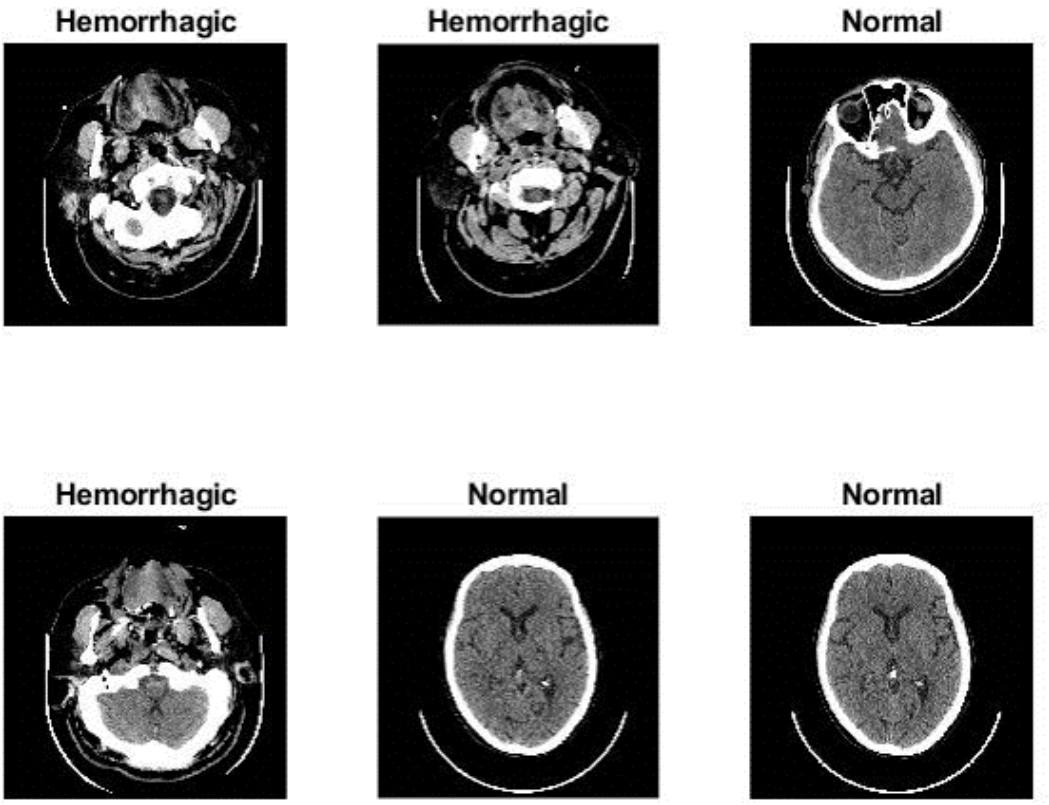

Figure 2. CT samples for the hemorrhage dataset.

3.2. Enhancement of CT Images

The image enhancement process is vital to obtaining high-quality images in the later stages. The resolution, reliability and interoperability reflect the quality of the images. Many factors affect the accuracy of CT images, including the patient's movement inside the scanner, reflections and the accuracy of different devices and the scanner. Unwanted or low signals destroy CT images. The field of bias in CT images is the differences in intensity from black to white. Thus, failure to correct the bias field will destroy the CT images, which leads to incorrect diagnostic results. Therefore, removing noise and correcting the bias field will result in high-resolution and reliable images. In this study, the mean RGB colors of CT images were tuned, and color consistency was achieved by adjusting the scaling. After that, the images were enhanced by two filters: the average filter to remove noise and increase the contrast of the images and the Laplacian filter to show the edges of the cerebral hemorrhage area [32]. First, the average filter is set to a size of 5×5 pixels, so a pixel will be selected at a time and replaced by an average of 24 adjacent pixels as described in Equation (1) [33]:

$$m(l) = \frac{1}{L} \sum_{i=0}^{L-1} z(l-1) \tag{1}$$

where $m(l)$ is the input, $z(l-1)$ is the previous input and L refers to the number of pixels in the image. Second, a Laplacian filter is applied to show the edges of the cerebral hemorrhage area and distinguish it from healthy brain areas, as described by Equation (2):

$$\bigtriangledown^2 \mathrm{f} = \frac{\partial^2 f}{\partial x^2} + \frac{\partial^2 f}{\partial y^2} \tag{2}$$

where $\bigtriangledown^2 f$ is a second-order differential operator, x and y are the coordinates of the matrix and ∂^2 indicates second-order partial derivatives.

Finally, the two enhanced images are merged. The reason for overlapping the two images to show a clearer enhanced image is because the image generated by the averaging filter increases the contrast of the images, while the Laplacian filter works to show the edges of the bleeding area. Thus, we find an improved bleeding area as described by Equation (3):

$$\text{Image enhanced} = m(l) - \bigtriangledown^2 f \tag{3}$$

Figure 3 shows a set of CT samples for hemorrhages after all dataset images have undergone enhancement.

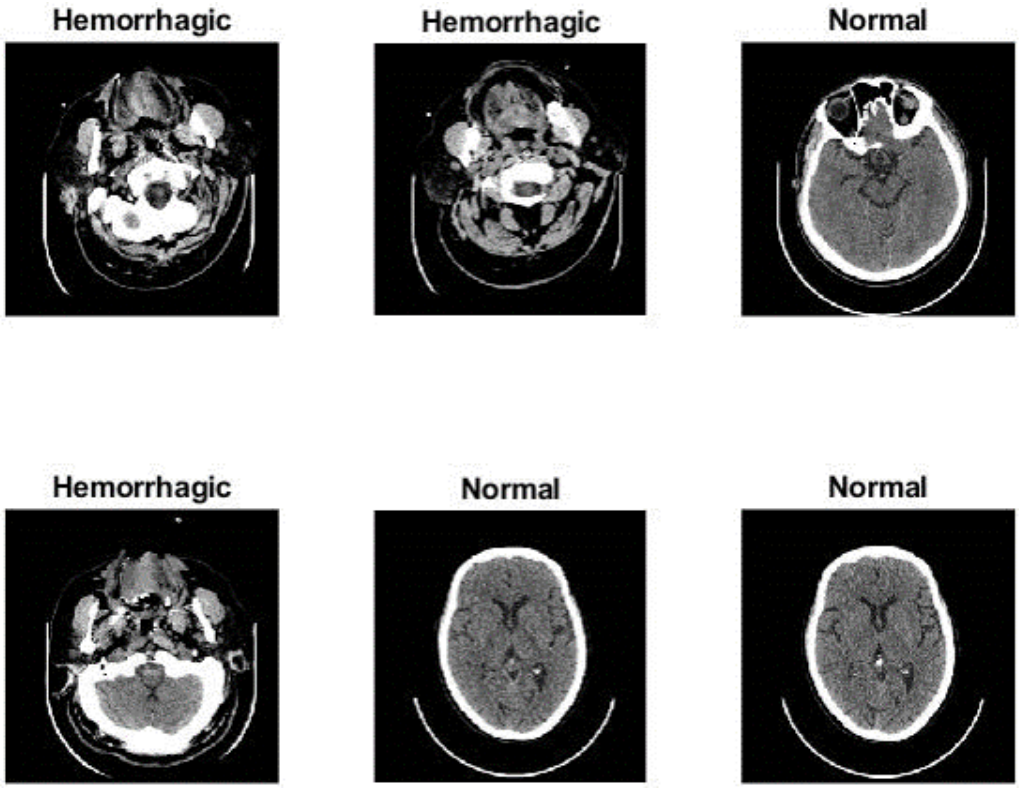

Figure 3. Set of CT images of a hemorrhage after image enhancement.

3.3. Deep Learning Models

Deep learning techniques are considered some of the most important artificial intelligence techniques to have entered many fields. Still, the complexity of their development and their high cost have strongly influenced their postponement and return in the past few years. These are helpful because they require huge amounts of data to classify items efficiently, but they require large computing resources, are expensive and take time to train. Deep learning networks are known as convolutional neural networks (CNNs). A CNN contains many 2D layers and thus is suitable technology for 2D image processing [14]. In general, a CNN's weights are filters that wrap around the image to process a specific task. Therefore, the specificity of these networks lies in the fact that each neuron receives connections from cells in the same layer and does not receive connections from the previous layers. Therefore, each layer is specialized for a specific task and reduces the number of weights and connections in the network.

CNNs are characterized by having many layers, and they eliminate the need to extract features manually. There is no need to specify features to classify them with one of the classification algorithms. A CNN trains the features and learns them during the training phase. Automatic feature extraction is what makes CNNs accurate and efficient for classification. CNN architectures show how the first layers extract lower-level features and

the subsequent layers extract deeper levels. Each layer increases the extraction of complex features. For example, the first layer can extract the edge features. In contrast, the next layer works to extract the geometric features of the object, and thus each convolutional layer performs a specific task.

CNNs consist of many layers, the most important of which are the following:

Convolutional Layer: CNNs contain many convolutional layers, and each layer has a specific task. Three parameters control this layer: the filter size, zero-padding and p-step. Each layer has a particular filter size and works in a particular way to wrap the filter $f(t)$ with a specific image size $x(t)$ [34]. The filter moves over all parts of the image, calculates the product of the filter with the target area of the image and then adds the values as described by Equation (4). Zero-padding preserves the size of the original image, and p-step determines the step size the filter moves with on the image:

$$\mathrm{y(t)} = (x \times f)(t) = \int x(a) f(t-a) da \tag{4}$$

where $f(t)$ is the filter, $x(t)$ is the image input and the output is represented by y(t).

Pooling layer: The pooling layers work to reduce the image dimensions, which reduces the computational cost in the later layers and reduces the parameters and connections used. There are two ways to reduce the dimensions: max pooling and average pooling. Each method has a specific mechanism of action. The average pooling layers determine a certain amount of the image according to the filter size. Then, the selected values are averaged [35]. All selected values are replaced with their average values as shown in Equation (5). The max pooling method defines a group of image pixels according to the filter size. Then, the max value is chosen and represented instead of the selected area in the image as described by Equation (6):

$$\mathrm{P(i,j)} = \frac{1}{k^2} \sum_{m,n=1\ldots k} A[(i-1)p+m, (j-1)p+n] \tag{5}$$

$$\mathrm{P(i,j)} = max_{m,n=1\ldots k} A[(i-1)p+m, (j-1)p+n] \tag{6}$$

where A is the number of pixels in the filter, m and n represents the matrix's dimensions, k is the size of the matrix and p is the step.

Fully Connected Layer: This is a layer connected to the last convolutional layer of a model which is responsible for converting data from bi-directional to unidirectional. It consists of thousands of neurons linked together. Finally, the softmax activation layer is responsible for attaching the label to the image to sort it into its appropriate class by applying the similarity probability.

There are also many auxiliary classes, such as the rectified linear unit (ReLU), which pass positive values but convert negative values to zero, as described in Equation (7):

$$\mathrm{ReLU(x)} = max(0, x) = \begin{cases} x, & x \geq 0 \\ 0, & x < 0 \end{cases} \tag{7}$$

The dropout layer overcomes the overfitting problem caused by millions of network parameters. Thus, this layer works to pass a certain amount of neurons in each repetition. In this study, the dropout layer was set to 50%, which means that the network passed 50% of the neuron's information on each iteration, but it doubled the model's training time. This study evaluated the CT images of the hemorrhage dataset with three deep learning models: GoogLeNet [36], ResNet-50 [15] and AlexNet [16]. Figure 4 describes the basic architecture of the pretrained GoogLeNet, ResNet-50 and AlexNet models for computed tomography evaluation for cerebral hemorrhage diagnosis.

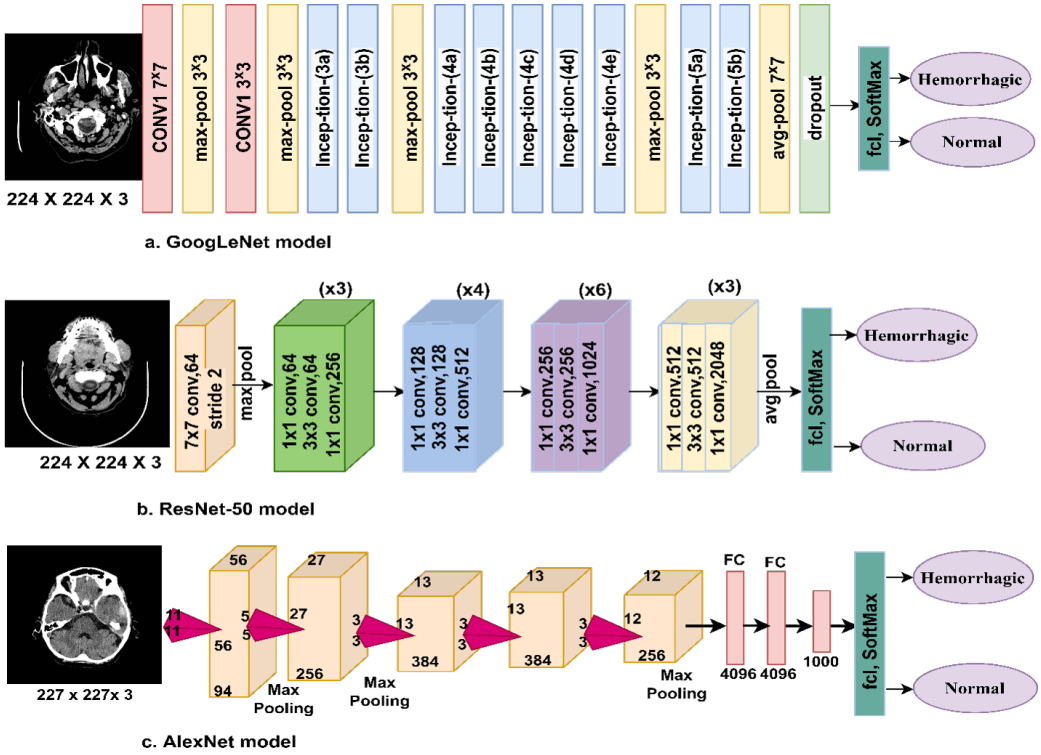

Figure 4. Infrastructure framework for CNN models for evaluating CT images for the diagnosis of cerebral hemorrhage disease.

3.4. Hybrid of Deep Learning and Machine Learning

In this section, a new technique is presented, namely a hybrid technology between the deep learning models applied in this study (GoogLeNet, ResNet-50 and AlexNet) with a machine learning (SVM) algorithm for CT image diagnosis for early and rapid detection of hemorrhages. CNNs require high specifications and costly computer resources, and training a dataset is very time-consuming, so these are challenges faced by CNN models. Therefore, hybrid techniques require medium-cost computer resources which are fast in training the dataset. Thus, this technique solves the challenges faced by CNN models. Hybrid methods consist of two blocks: CNN models and SVM algorithms. The first block (GoogLeNet, ResNet-50 and AlexNet) receives the enhanced CT images, extracts the deep feature maps, and sends them to the second block [37]. The second block receives the feature maps and classifies them with high accuracy and efficiency by the SVM algorithm. Figure 5a–c shows the methodology of the hybrid techniques which is noted to consist of two blocks, called GoogLeNet + SVM, ResNet-50 + SVM and AlexNet + SVM, for CT image diagnosis for early detection of hemorrhages.

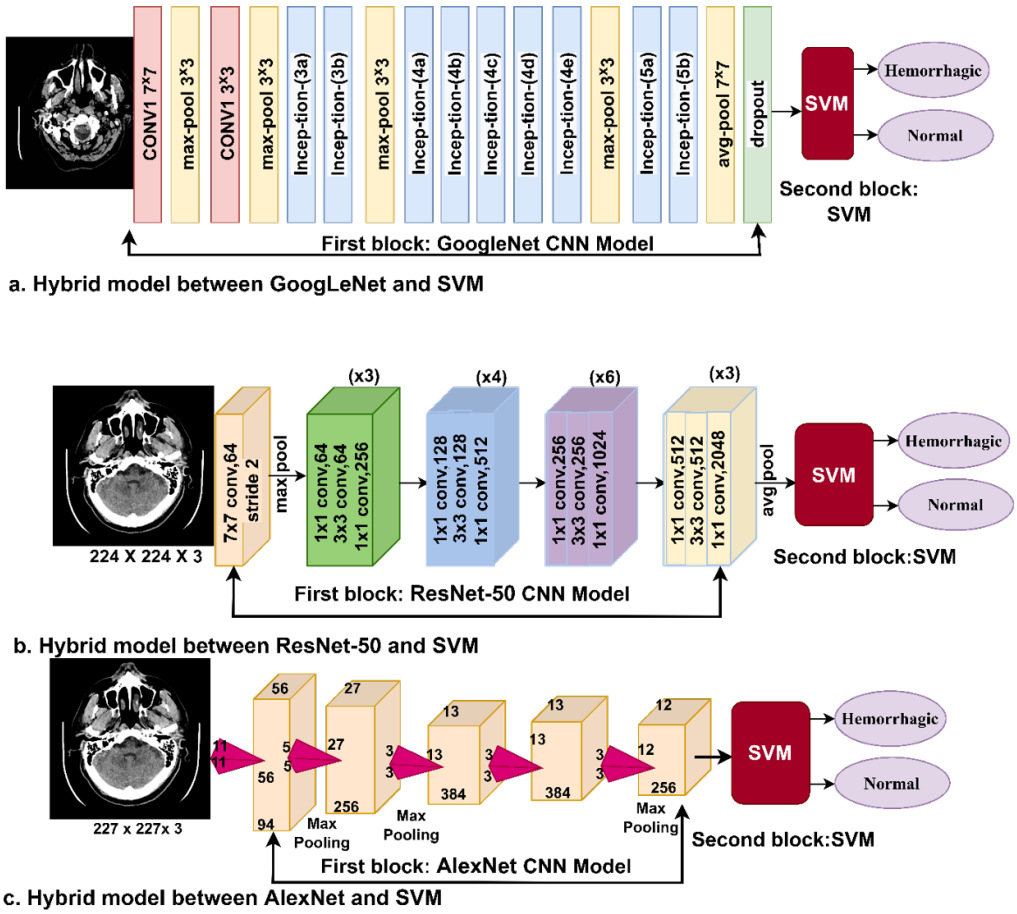

Figure 5. Hybrid methodology between deep learning and SVM. (**a**) GoogleNet+SVM. (**b**) ResNet-50 + SVM. (**c**) AlexNet + SVM.

3.5. Combining the Features of Deep Learning with Traditional Algorithms

This section presents a hybrid technology similar to that in the previous section. Still, this technique is characterized by the fusion of features extracted by CNN models (GoogLeNet, ResNet-50 and AlexNet) with hybrid features extracted by GLCM and LBP algorithms. This proposed method is characterized by its requirement of medium-cost computer resources and its speed in training the dataset. The mechanism of the proposed system is as follows. First, the CT images are fed to the CNN models, where each model extracts the feature maps and stores them in a feature vector so that each image contains 4096 features. Therefore, the dataset is represented in a matrix of features with a size of 7032 $\times$ 4096. Due to the high-dimensional features, the features matrix is fed to the PCA algorithm [38] to reduce the dimensions and choose the essential representative features for each image. Then, the features matrix becomes 7032 $\times$ 1024 in size.

After the improvement, the hemorrhagic area is divided and separated from the healthy part. Extracting the features from the entire image leads to extracting features for the affected and healthy parts and leads to inaccurate diagnostic results. This method is considered one of the most critical and complex image processing methods. In this study, the adopted region growth algorithm was used. The algorithm groups similar pixels so that the pixels of each region are the same. The algorithm is based on an incremental approach so that the image is divided into many regions, each region starts with one pixel, and then each region grows gradually by collecting similar pixels in one region. Thus, the algorithm continues until each pixel is assigned to its own region, and there cannot be similar pixels in two regions. The process continues until the segmentation is completed and the region of interest is obtained.

After the fragmentation process, tiny holes are left in the regions of interest that do not belong to the region of interest. Therefore, applying the morphological method is one of the ways to improve the images after the segmentation process to obtain more enhanced images. The method searches for holes in the region of interest. It treats them according to many operations such as opening, closing, erosion and dilation based on wrapping the structure element around the image.

The third step is the application of GLCM and LBP algorithms to extract features from the lesion area. The GLCM algorithm produces 13 statistically features [39], while the LBP algorithm produces 203 features [40]. Then, the features of the two algorithms are combined into one feature vector so that each vector represents 216 features. Thus, the dataset becomes represented in the feature matrix with a size of 7032 × 216. Fourth, the resulting features from CNN models after dimensionality reduction are combined with the features extracted by the GLCM and LBP algorithms and stored in a new feature matrix so that its size becomes 7032 × 1240. Fifth, the hybrid features between the CNN models and the (GLCM and LBP) algorithms are fed to an ANN for classifying them with higher accuracy and efficiency than the other proposed methods. Figure 6 shows the basic structure and methodology of extracting features using CNN models and GLCM and LBP algorithms, merging them and then feeding them to the ANN algorithm for classification. This method is one of our main contributions to this study.

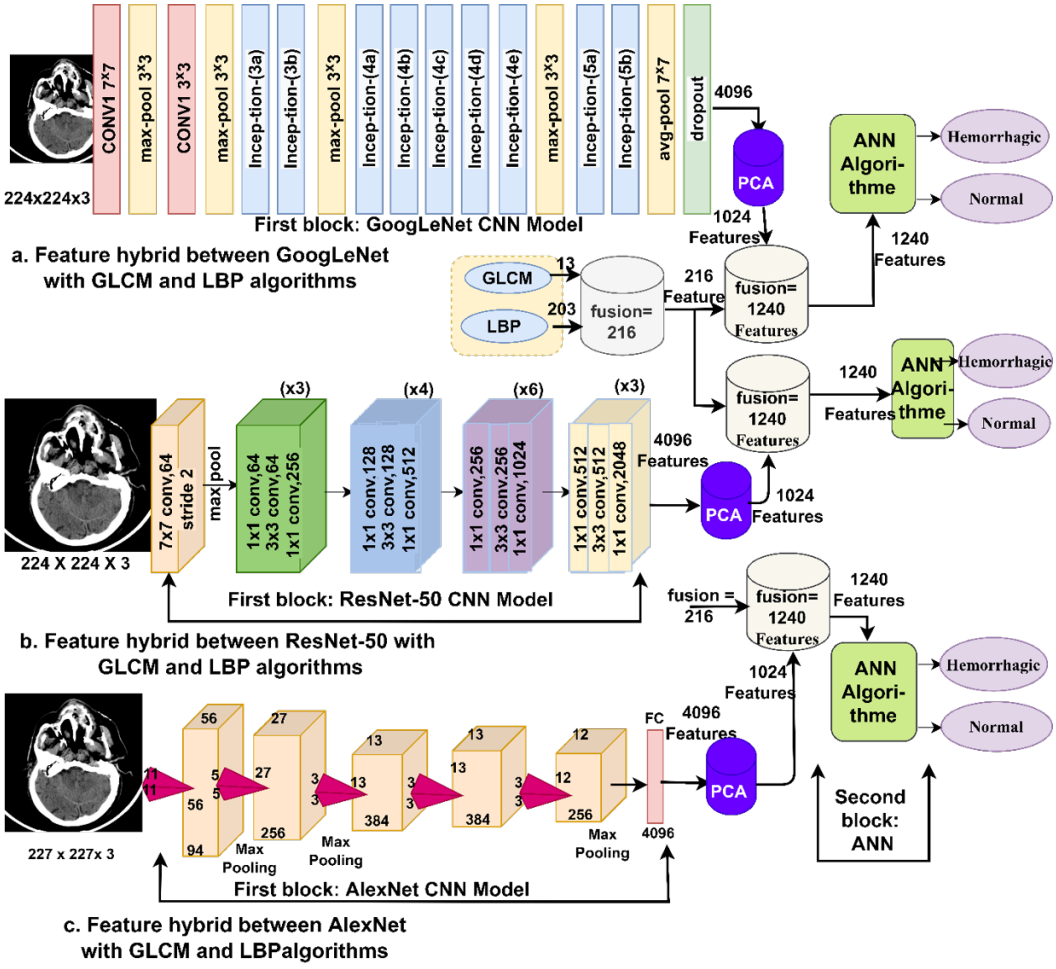

Figure 6. Basic methodology of hybrid feature extraction technique between CNN models and GLCM and LBP algorithms and their classification by an ANN.

4. Experimental Results

4.1. Splitting Dataset and Environment Set-Up

The performance of all proposed networks was evaluated on the same CT images of the hemorrhage dataset. The dataset consists of 7032 CT images divided into two categories: hemorrhage and non-hemorrhage. The dataset was split at the subject level during the training, validation and testing phases. Table 1 summarizes the breakdown of the data set during all phases, splitting into 80% for the training and validation phases (80:20) and 20% for the testing phase. First, for the cerebral hemorrhage category, 14 subjects (patients) suffering from a cerebral hemorrhage, representing 2152 CT images, were allocated for the training and validation phase, and four subjects (patients) with cerebral hemorrhages represented 537 CT images for the testing phase. Second, for the healthy images, 22 subjects were allocated to patients without cerebral hemorrhages, which represented 3474 CT images for the training and validation phase, and five subjects were for patients without cerebral hemorrhages, which represented 869 CT images for the testing phase. A MATLAB 2018b operating environment implemented the proposed systems in this study with Intel® i5 6th generation computer specifications, with 12 GB RAM and a 4-GB GPU.

Table 1. Splitting of the hemorrhage dataset for the training, validation and testing phases.

Phase	Training and Validation (80:20)		20% for Testing
Classes	**80% for Training**	**20% for Validation**	
Hemorrhage	1722	430	537
Non-hemorrhage	2779	695	869

4.2. Evaluation Metrics

All methods proposed in this study were evaluated with the same measures—accuracy, precision, sensitivity, specificity, and AUC—for diagnosing the CT images of the hemorrhage dataset. Equations (8)–(11) illustrate the performance of the proposed systems [41,42]. It is noted that the equations contain variables that represent correctly and incorrectly classified images. The equations' variables were obtained from the confusion matrix produced by all the proposed systems. A confusion matrix is a tool for assessing the performance of systems on the hemorrhage dataset. The confusion matrix contains all samples of the dataset, either correctly classified as *TP* or *TN* or incorrectly classified as *FP* or *FN*:

$$\text{Accuracy} = \frac{TN + TP}{TN + TP + FN + FP} \times t100\% \quad (8)$$

$$\text{Precision} = \frac{TP}{TP + FP} \times 100\% \quad (9)$$

$$\text{Sensitivity} = \frac{TP}{TP + FN} \times 100\% \quad (10)$$

$$\text{Specificity} = \frac{TN}{TN + FP} \times 100\% \quad (11)$$

where true positive (*TP*) is the number of correctly classified hemorrhage CT images, true negative (*TN*) is the number of correctly classified non-hemorrhage CT images, false positive (*FP*) is the number of CT images that are not hemorrhages but are classified as hemorrhages, and false negative (*FN*) is the number of hemorrhage CT images classified as non-hemorrhage CT images.

The AUC is the area under the curve of the ROC plot, which is defined as the true positive rate against the false positive rate at various threshold values.

4.3. Results of the Deep Learning

This section presents the performance results of the pretrained GoogLeNet, ResNet-50 and AlexNet models. In these methods, pretrained models were used on the ImageNet database, which contains more than 1 million images for more than 1000 classes but does not contain a hemorrhage dataset, and thus the transfer learning technique was used. Transfer learning is the CNN models' acquired experience to perform new tasks (classification of the hemorrhage dataset). For high-efficiency performance, CNN models require a large dataset, which is not available, especially in medical image datasets. Thus, CNN models face the problem of overfitting during the training phase, and therefore this challenge can be solved by using the data augmentation method. The data augmentation method increases each image in the dataset artificially and by a specified amount in many operations, such as rotation, shifting, flipping and cropping [43]. In addition, this method helps solve the problem of the unbalanced dataset, as it increases the class of the minority by an amount more than that of the majority. In this study, Table 2 summarizes the dataset before and after applying the data increase during the training phase, where it is noted that the hemorrhage class increased each image by five times, while in the non-hemorrhage class, each image increased by three times, which means obtaining a nearly balanced dataset during the training stage.

Table 2. Using the data augmentation method to overcome the overfitting and balancing of the dataset.

Name of Class	Hemorrhage	Non-Hemorrhage
Without augmentation	1722	2779
With augmentation	8605	8337

Table 3 summarizes the training options for the GoogLeNet, ResNet-50 and AlexNet models during the training phase. In this study, the training options were tested and changed many times until the training options were set as shown in the table, which was the best training option. As such, the models reached the best evaluative results for the hemorrhage dataset CT images. It is noted from the table that the optimizer option was chosen, in addition to setting the initial learn rate, validation frequency, mini batch size, execution environment and time spent to train the dataset.

Table 3. Set training options for GoogLeNet, ResNet-50 and AlexNet models.

Options	GoogLeNet	ResNet-50	AlexNet
Training Options	adam	adam	adam
Mini Batch Size	18	10	120
Max Epochs	3	6	10
Initial Learn Rate	0.0003	0.0001	0.0001
Validation Frequency	3	5	50
Training Time (min)	347 min 14 s	221 min 38 s	57 min 13 s
Execution Environment	GPU	GPU	GPU

The GoogLeNet, ResNet-50 and AlexNet models produced promising results in evaluating the CT images to make a diagnosis of the hemorrhage dataset. Table 4 summarizes the results achieved by all the proposed models. It is noted that all models were good at evaluating the CT images to make a diagnosis that helps doctors and experts in the rapid diagnosis of intracranial hemorrhages, as this is a sensitive disease that needs a proper diagnosis and prompt and appropriate treatment. It is also noted that GoogLeNet is slightly superior to other networks. The GoogLeNet model achieved an accuracy of 94%, precision of 93.53%, sensitivity of 93.48%, specificity of 93.87% and AUC of 96.82%. In contrast, the ResNet-50 model achieved an accuracy of 91.7%, precision of 91.1%, sensitivity of 92.34%, specificity of 92.44% and AUC of 95.76%. In contrast, the AlexNet model achieved an

accuracy of 91.5%, precision of 93.31%, sensitivity of 90.41%, specificity of 91.17% and AUC of 97.12%.

Table 4. Evaluative results of diagnosed CT images of hemorrhage dataset using GoogLeNet, ResNet-50 and AlexNet.

Measure	GoogLeNet	ResNet-50	AlexNet
Accuracy (%)	94	91.7	91.5
Precision (%)	93.53	91.1	93.31
Sensitivity (%)	93.48	92.34	90.41
Sepecificy (%)	93.87	92.44	91.17
AUC (%)	96.82	95.76	97.12

Figure 7 shows the performance of the GoogLeNet, ResNet-50, and AlexNet models for early hemorrhage diagnosis CT images in graph form.

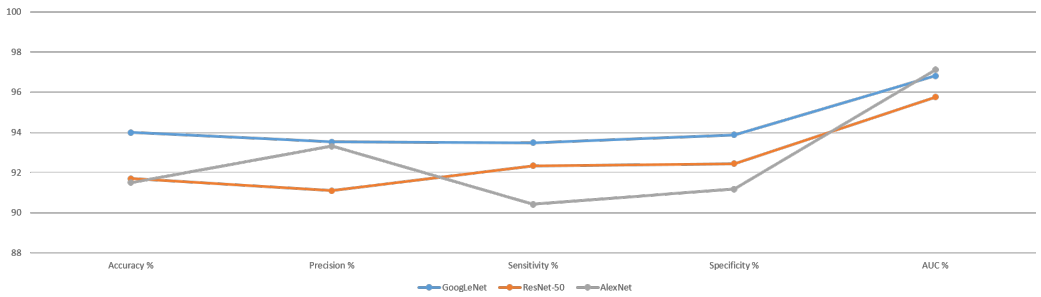

Figure 7. Performance of CNN models for diagnosing the hemorrhage dataset.

Figure 8 shows the performance of the GoogLeNet model for evaluating CT images for the rapid diagnosis of the hemorrhage dataset, where it is noted that the system reached an overall accuracy of 94% and an accuracy of 92% for diagnosing hemorrhage images. In contrast, it achieved an accuracy of 95.3% for diagnosing non-hemorrhage images. The model also reached an AUC of 96.82%.

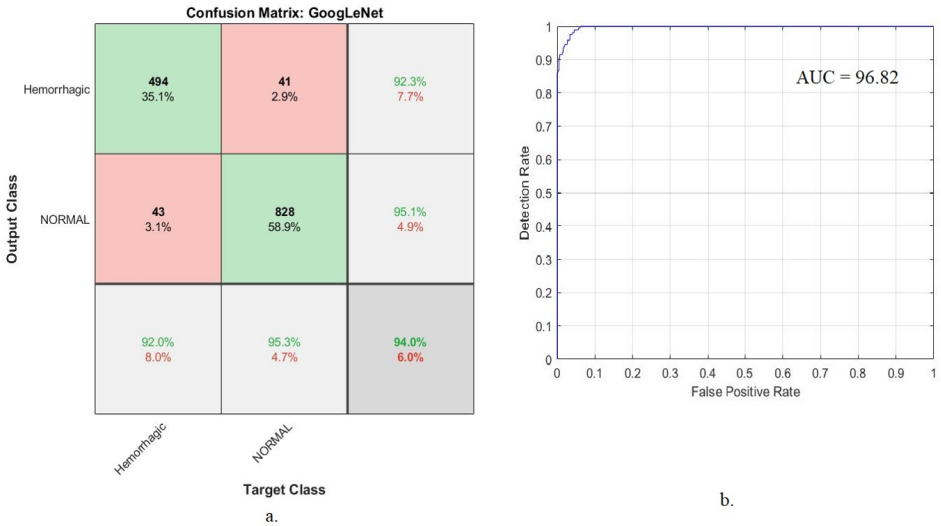

Figure 8. Performance of the GoogLeNet model for diagnosing hemorrhage dataset. (**a**) Confusion matrix. (**b**) AUC.

It is noted from the figure that there were CT images that were incorrectly classified, where 43 images of the hemorrhagic class were incorrectly classified as non-hemorrhagic.

In comparison, 41 images of the non-hemorrhagic class were incorrectly classified as hemorrhagic.

Figure 9 shows the performance of the ResNet-50 model for evaluating CT images for the rapid diagnosis of the hemorrhage dataset, where it is noted that the system reached an overall accuracy of 91.7% and an accuracy of 93.1% for diagnosing hemorrhage images. In contrast, it achieved 90.8% for diagnosing non-hemorrhage images, and the model also reached an AUC of 95.76%.

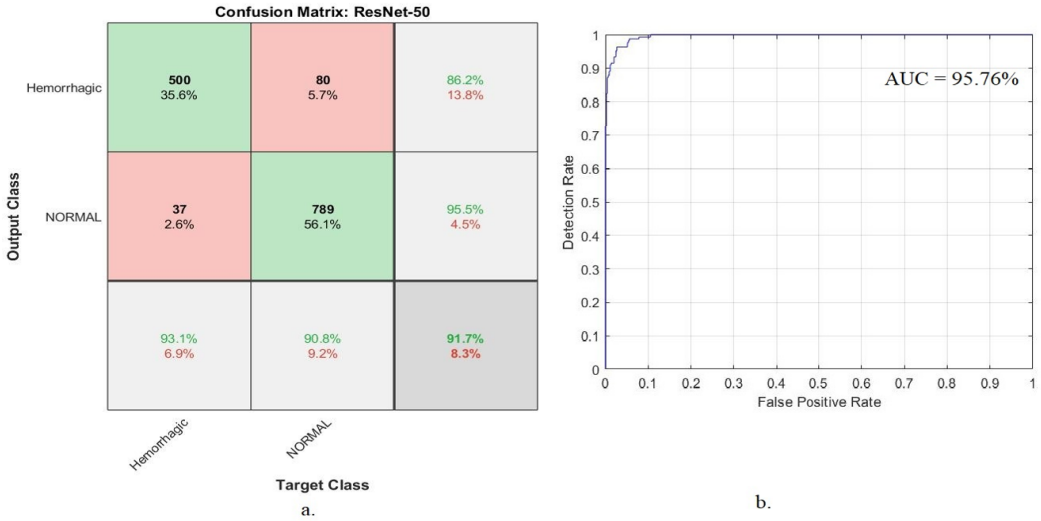

Figure 9. Performance of the ResNet-50 model for diagnosing the hemorrhage dataset. (**a**) Confusion matrix. (**b**) AUC.

It is noted from the figure that there were CT images that were incorrectly classified, where 37 images of the hemorrhagic class were incorrectly classified as non-hemorrhagic. In comparison, 80 images of the non-hemorrhagic class were incorrectly classified as hemorrhagic.

The AlexNet model reached an overall accuracy of 91.5%, and it reached an accuracy of 79.1% for diagnosing hemorrhage images. In contrast, it achieved an accuracy of 99.1% for diagnosing non-hemorrhage images. The system also reached an AUC of 97.12% for evaluating CT images for rapid diagnosis of the hemorrhage dataset, as shown in Figure 10.

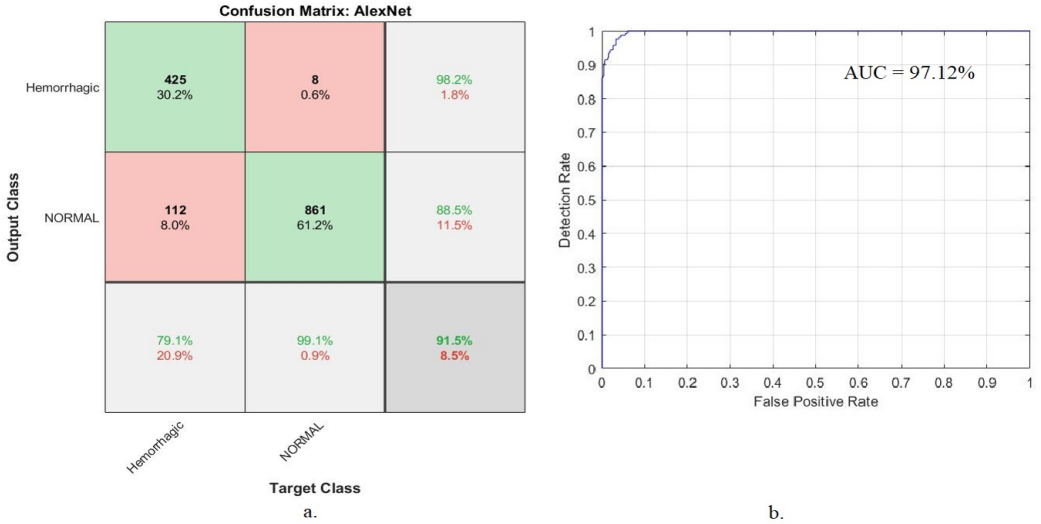

Figure 10. Performance of the AlexNet model for diagnosing the hemorrhage dataset. (**a**) Confusion matrix. (**b**) AUC.

It is noted from the figure that there were CT images that were incorrectly classified, where 112 images of the hemorrhagic class were incorrectly classified as non-hemorrhagic. In comparison, eight images of the non-hemorrhagic class were incorrectly classified as hemorrhagic.

4.4. Results of Hybrid Deep Learning with the SVM Algorithm

This section discusses the performance of hybrid techniques between the deep learning networks (GoogLeNet, ResNet-50 and AlexNet) and the SVM algorithm for CT image diagnosis for rapid detection of the hemorrhage dataset. There are many reasons for applying this technique: its requirements for medium specification computer resources, its speed in training the dataset and its efficiency in super-diagnostics. This technique consists of two blocks: deep learning models and the SVM. Deep learning models extract the deep feature maps and send them to the SVM algorithm to classify them with high accuracy.

Table 5 summarizes the performance of the hybrid techniques, namely GoogLeNet + SVM, ResNet-50 + SVM and AlexNet + SVM, for evaluating CT images for rapid diagnosis of intracranial hemorrhages. It is noted that the GoogLeNet + SVM system was slightly superior to the rest of the systems. The GoogLeNet + SVM network reached an accuracy of 97.4%, precision of 97.43%, sensitivity of 97.38%, specificity of 98.1% and AUC of 98.74%. At the same time, the ResNet-50 + SVM network reached an accuracy of 97.2%, precision of 97.13%, sensitivity of 96.89%, specificity of 98.67% and AUC of 98.51%. Additionally, the AlexNet + SVM network reached an accuracy of 95.7%, precision of 96.23%, sensitivity of 95.5%, specificity of 96.18% and AUC of 99.14%.

Table 5. Evaluative results of diagnosed CT Images of hemorrhage dataset using GoogLeNet + SVM, ResNet-50 + SVM and AlexNet + SVM.

Measure	GoogLeNet + SVM	ResNet-50 + SVM	AlexNet + SVM
Accuracy (%)	97.4	97.2	95.7
Precision (%)	97.43	97.13	96.23
Sensitivity (%)	97.38	96.89	95.5
Sepecificy (%)	98.1	98.67	96.18
AUC (%)	98.74	98.51	99.14

Figure 11 shows the performance of the proposed hybrid techniques for interpreting CT images to make a diagnosis of a hemorrhage dataset in graph form.

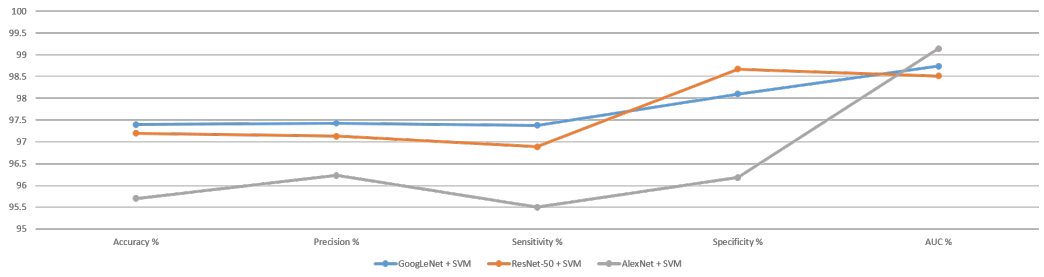

Figure 11. Performance of hybrid technique for diagnosing the hemorrhage dataset.

The performance of hybrid systems was evaluated using the confusion matrix. The confusion matrix summarizes all samples of the dataset that were correctly classified and those that were incorrectly classified and then produces the overall accuracy and diagnostic accuracy for each class.

Figure 12 shows the evaluation of the CT images using the GoogLeNet + SVM network for rapid diagnosis of the hemorrhage dataset. It is noted that the system reached an overall accuracy of 97.4% and, for diagnosing hemorrhage images, an accuracy of 95.9%. In

contrast, it achieved up to 98.3% accuracy for diagnosing non-hemorrhage images. The model also reached an AUC of 98.74%.

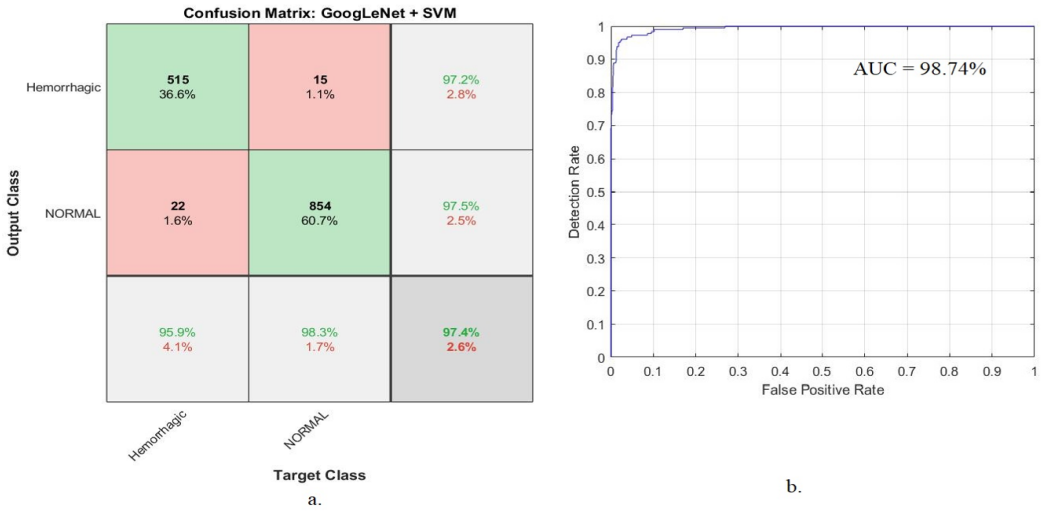

Figure 12. Performance of the GoogleLeNet + SVM model for diagnosing the hemorrhage dataset. (**a**) Confusion matrix. (**b**) AUC.

It is noted from the figure that there were CT images that were incorrectly classified, where 22 images of the hemorrhagic class were incorrectly classified as non-hemorrhagic. In comparison, 15 images of the non-hemorrhagic class were incorrectly classified as hemorrhagic.

The ResNet-50 + SVM network reached an overall accuracy of 97.2%, and for diagnosing hemorrhage images, its accuracy was 96.8%. In contrast, it achieved 97.4% accuracy in diagnosing non-hemorrhage images. The system also reached an AUC of 98.51% for evaluating CT images for rapid diagnosis of the hemorrhage dataset, as shown in Figure 13.

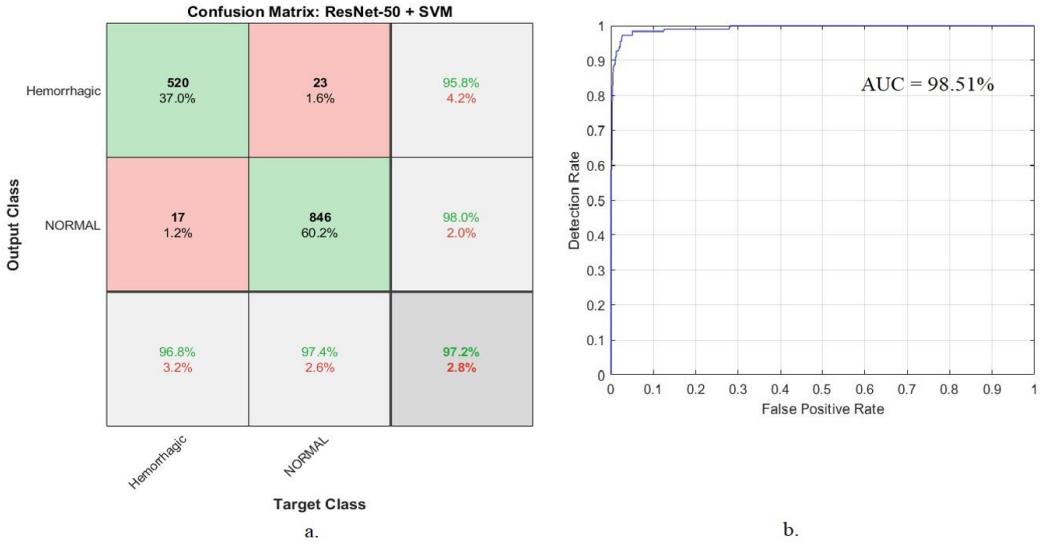

Figure 13. Performance of the ResNet-50 + SVM model for diagnosing the hemorrhage dataset. (**a**) Confusion matrix. (**b**) AUC.

It is noted from the figure that there were CT images that were incorrectly classified, where 17 images of the hemorrhagic class were incorrectly classified as non-hemorrhagic. In comparison, 23 images of the non-hemorrhagic class were incorrectly classified as hemorrhagic.

Figure 14 shows the performance of the AlexNet + SVM network for evaluating the CT image for rapid diagnosis of the hemorrhage dataset, where it is noted that the system

reached an overall accuracy of 95.7% and an accuracy of 94.2% for diagnosing hemorrhage images. In contrast, it achieved an accuracy of 96.5% for the diagnosis of non-hemorrhage images. The model also reached an AUC of 99.14%.

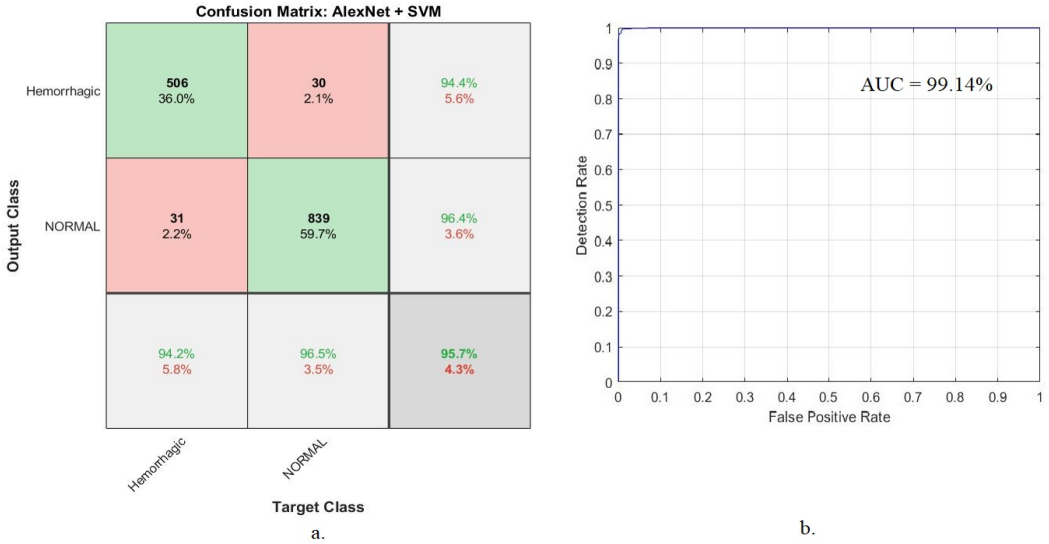

Figure 14. Performance of the AlexNet + SVM model for diagnosing the hemorrhage dataset. (**a**) Confusion matrix. (**b**) AUC.

It is noted from the figure that there were CT images that were incorrectly classified, where 31 images of the hemorrhagic class were incorrectly classified as non-hemorrhagic. In comparison, 30 images of the non-hemorrhagic class were incorrectly classified as hemorrhagic.

4.5. Results of the Hybrid Feature Deep Learning with the GLCM and LBP Algorithms

This section introduces a new technique that combines features extracted by CNN models and the GLCM and LBP algorithms, combines all features and classifies them with the ANN algorithm. This proposed method diagnoses CT images accurately and quickly because the intracranial hemorrhage's treatment cannot be delayed.

The hemorrhage dataset was divided into 63.3% for training, 16% for validation and 20.7% for testing. The algorithm was trained several times, and its performance was set at the best performance. The algorithm achieved the best performance when adjusting the number of hidden layers to 20 hidden layers. The performance of the proposed system was evaluated by several evaluation tools, as illustrated below.

4.5.1. Best Validation Performance

The mean square error or cross-entropy is one tool that evaluates the ANN network of the hemorrhage dataset. The dataset goes through many epochs, and in each epoch, a cross-entropy (mean square error) is obtained during all phases (training, validation and testing) to evaluate the ANN algorithm. The algorithm continues until it reaches the minimum mean square error between the expected and actual output. Figure 15 shows the performance of the ANN algorithm on the hemorrhage dataset during the training phase, represented by the blue color, the test phase, represented by the red color, and the validation phase, represented by the green color. It is noted that the algorithm reached the best performance (i.e., reached the minimum error between the expected and actual values) at the best validation performance of 0.0005904 at epoch 34, 0.0027462 at epoch 21 and 0.00087469 at epoch 25 based on the hybrid features of GoogLeNet + (GLCM and LBP), ResNet-50 + (GLCM and LBP) and AlexNet + (GLCM and LBP), respectively.

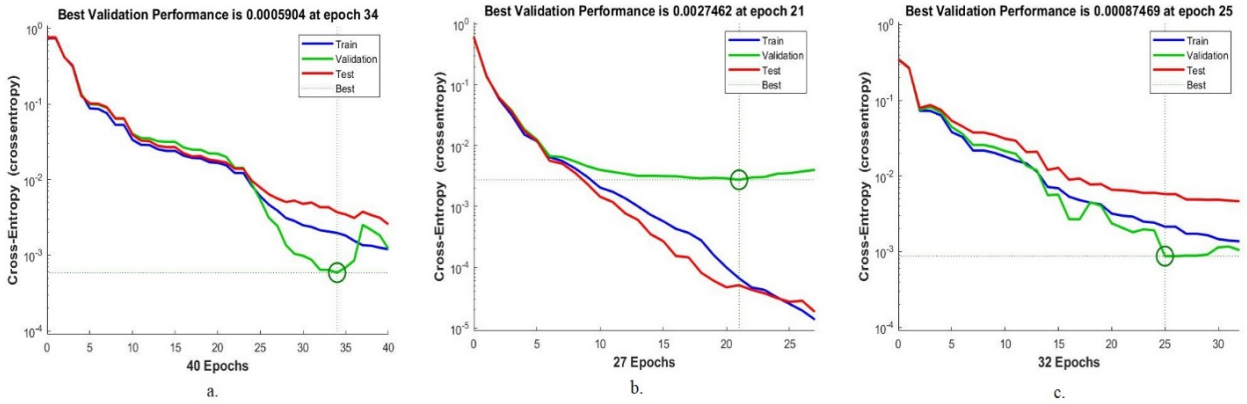

Figure 15. Best performance of ANN on hemorrhage dataset based on hybrid features by (**a**) GoogLeNet and GLCM + LBP, (**b**) ResNet-50 and GLCM + LBP and (**c**) AlexNet and GLCM + LBP.

4.5.2. Error Histogram

The error histogram is one of the tools used to evaluate the performance of the ANN network of CT images of a hemorrhage dataset. The ANN network evaluated the dataset during the training phase, represented by the blue histogram bin, the validation phase, represented by the green histogram bin, and the testing phase, represented by the red histogram bin. The algorithm continued until it reached the minimum error between the target values and the output. The orange color represents the best network performance. Figure 16 shows the error histogram of the ANN algorithm for the hemorrhage dataset, where the best network performance was observed between bins −0.9499 and 0.9499 when fed to the network by both methods (GoogLeNet + (GLCM and LBP)), and for ResNet-50 + (GLCM and LBP), it was observed between bins −0.9482 and 0.9482. When fed to the ANN algorithm by AlexNet + (GLCM and LBP), the best network performance was observed between bins −0.9492 and 0.9492.

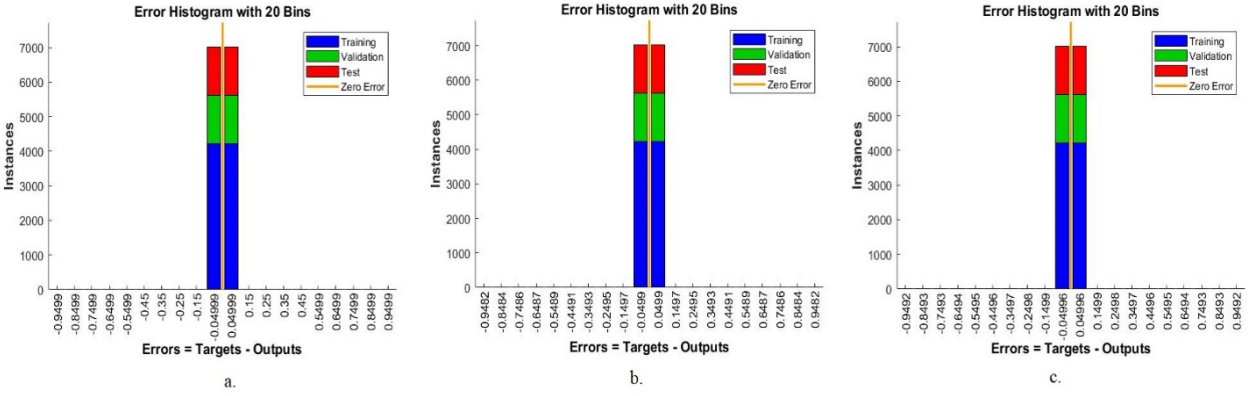

Figure 16. Error histogram of ANN on hemorrhage dataset based on hybrid features by (**a**) GoogLeNet and GLCM + LBP, (**b**) ResNet-50 and GLCM + LBP and (**c**) AlexNet and GLCM + LBP.

4.5.3. Receiver Operating Characteristic (ROC)

The ROC curve is one of the essential tools for measuring the classification performance of any binary classifier, because it illustrates its diagnostic ability as the discrimination threshold is varied. Specifically, the ROC curve is the plot of the true positive rate (or sensitivity on the *y*-axis) against the false positive rate (or 1-specificity on the *x*-axis) at various threshold values. The closer the ROC curve gets to the top left corner, the better the classifier is. The ROC curve was used to evaluate the performance of the ANN by computing the AUC during the training, validation and testing phases. Figure 17 describes the performance of the ANN for evaluating the dataset during all stages. The ANN reached a total AUC of 98.74%, 98.51% and 99.14% based on the hybrid features of

GoogLeNet + (GLCM and LBP), ResNet-50 + (GLCM and LBP) and AlexNet + (GLCM and LBP), respectively.

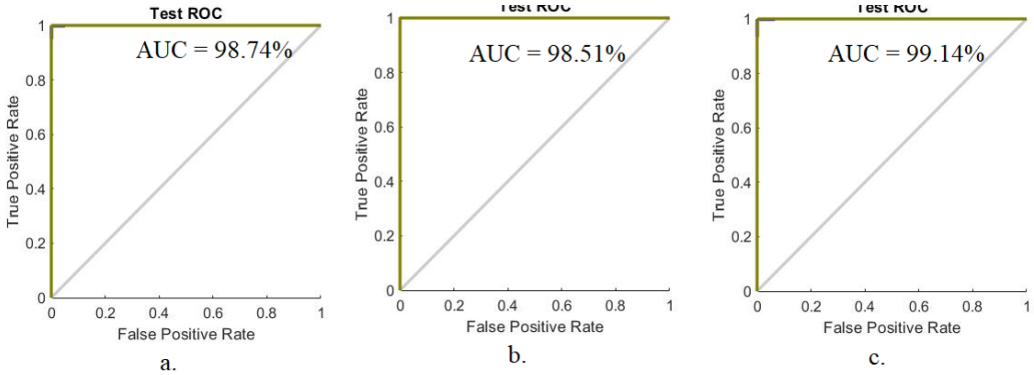

Figure 17. ROC of ANN on hemorrhage dataset based on hybrid features by (**a**) GoogLeNet and GLCM + LBP, (**b**) ResNet-50 and GLCM + LBP and (**c**) AlexNet and GLCM + LBP.

4.5.4. Confusion Matrix

The confusion matrix is the essential standard tool for evaluating the performance of systems. In this study, the ANN network was fed with three feature matrixes. Each feature matrix was the hybrid feature between one of the CNN (GoogLeNet, ResNet-50 and AlexNet) models and the features extracted by the GLCM and LBP algorithms.

Table 6 summarizes the performance of the feature hybrid, namely GoogLeNet deep features + (GLCM and LBP), ResNet-50 deep features + (GLCM and LBP) and AlexNet deep features + (GLCM and LBP), for evaluating CT images for rapid diagnosis of intracranial hemorrhages. When fed to the ANN using GoogLeNet feature + (GLCM and LBP), it achieved an accuracy of 98.9%, precision of 99.17%, sensitivity of 98.95, specificity of 99.36% and AUC of 99.58%. At the same time, when fed to the ANN using ResNet-50 feature + (GLCM and LBP), it achieved an accuracy of 99.1%, precision of 99.51%, sensitivity of 99.32%, specificity of 99.41% and AUC of 99.62%. Additionally, when fed to the ANN using the AlexNet feature + (GLCM and LBP), it achieved an accuracy of 99.3%, precision of 99.36%, sensitivity of 99.5%, specificity of 99.57% and AUC of 99.84%.

Table 6. Performance of ANN through hybrid features for early detection of hemorrhages.

Method of Combining Features	GoogLeNet Feature Map + (GLCM) and LBP	ResNet-50 Feature Map + (GLCM) and LBP	AlexNet Feature Map + (GLCM and LBP)
Accuracy (%)	98.9	99.1	99.3
Precision (%)	99.17	99.51	99.36
Sensitivity (%)	98.95	99.32	99.5
Specificity (%)	99.36	99.41	99.57
AUC (%)	99.58	99.62	99.84

Figure 18 shows the performance of the ANN network based on the hybrid features extracted from the CNN models and GLCM and LBP algorithms for computed tomography image diagnosis of the hemorrhage dataset in graph form.

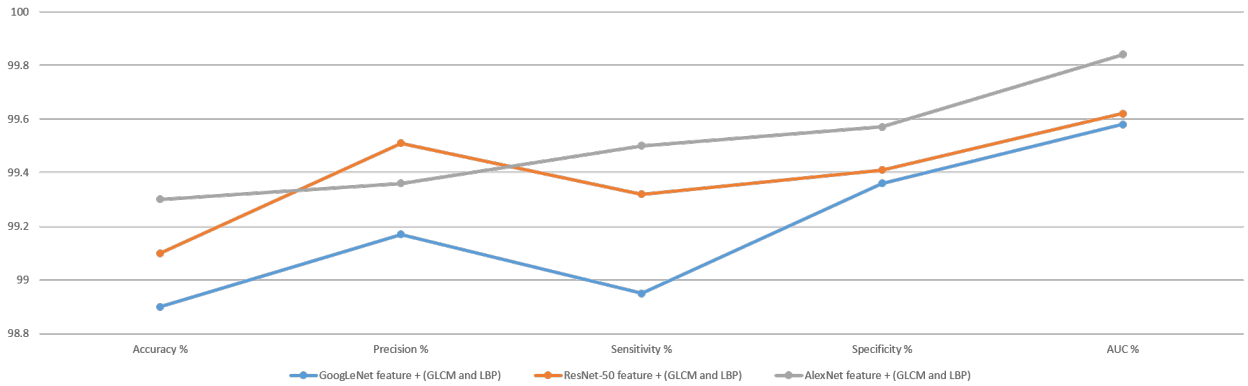

Figure 18. Performance of the ANN network based on hybrid features extracted.

Figure 19 shows the confusion matrix produced using the ANN algorithm to evaluate the features extracted by the GoogLeNet model with the hybrid features of the GLCM and LBP algorithms. The algorithm achieved superior results in evaluating the CT images to make a diagnosis of the hemorrhage dataset during the training, validation and testing phases. The network reached the following overall results. It is noted that the network reached an overall accuracy of 98.9% and an accuracy of 98.5% for diagnosing the hemorrhage images, and in contrast, it achieved an accuracy of 99.2% for diagnosing the non-hemorrhage images.

Figure 19. ANN's confusion matrix based on features fused between GoogLeNet and GLCM and LBP.

It is noted from the figure that there were CT images that were incorrectly classified, where eight images of the hemorrhagic class were incorrectly classified as non-hemorrhagic. In comparison, seven images of the non-hemorrhagic class were incorrectly classified as hemorrhagic.

Figure 20 shows the confusion matrix obtained using the ANN algorithm to evaluate the features extracted by ResNet-50 with the hybrid features from GLCM and LBP

algorithms. The network achieved superior results in evaluating the CT images to make a diagnosis of the hemorrhage dataset during all phases. The network reached the following overall results. It is noted that the network reached an overall accuracy of 99.1% and an accuracy of 98.1% for diagnosing the hemorrhage images. In contrast, it achieved an accuracy of 99.8% for diagnosing the non-hemorrhage images.

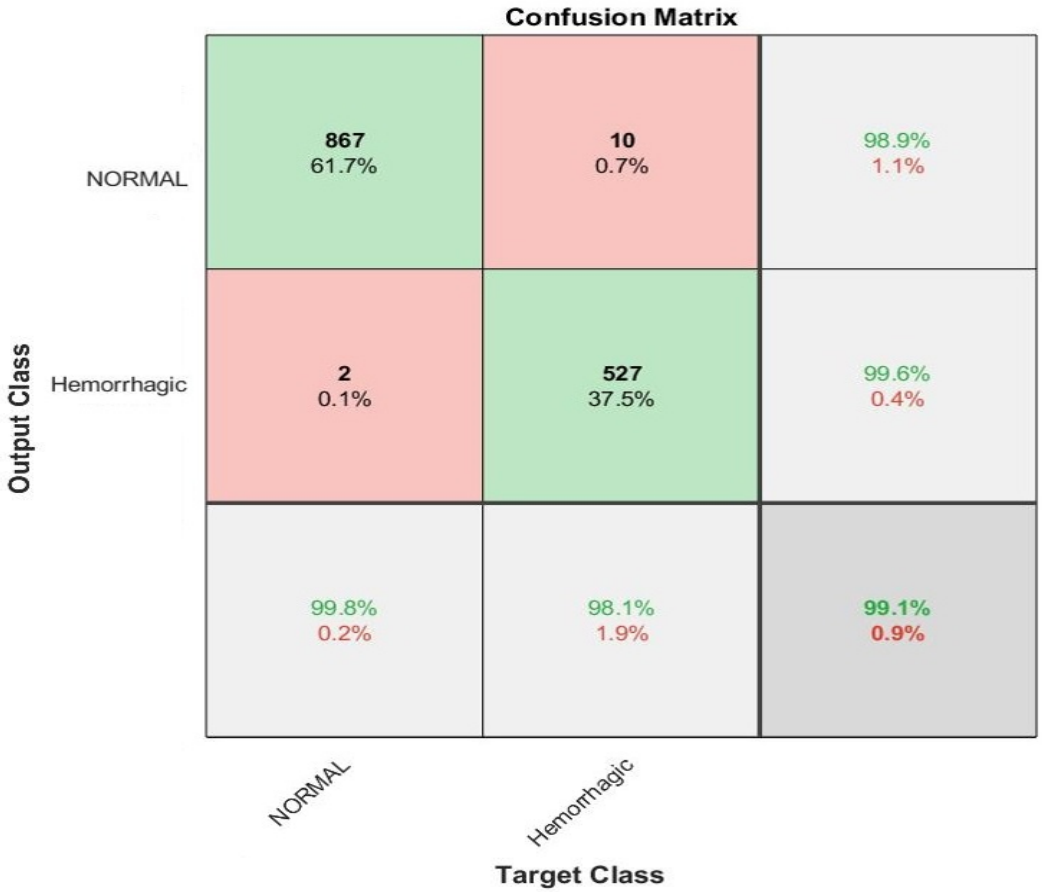

Figure 20. ANN's confusion matrix based on features fused between ResNet-50 and GLCM and LBP.

It is noted from the figure that there are CT images that are incorrectly classified, where ten images of the hemorrhagic class are incorrectly classified as non-hemorrhagic. In comparison, two images of the non-hemorrhagic class are incorrectly classified as hemorrhagic.

Figure 21 shows the confusion matrix produced using the ANN algorithm to evaluate the features extracted by the AlexNet model with the hybrid features of the GLCM and LBP algorithms. The network achieved superior results in evaluating CT images to make a diagnosis of the hemorrhage dataset during all phases. The network reached overall results, where it is noted that the network reached an overall accuracy of 99.3%; and an accuracy of 98.9% for diagnosing hemorrhage images. In contrast, it achieved an accuracy of 99.5% for diagnosing non-hemorrhage images.

It is noted from the figure that there are CT images that are incorrectly classified, where six images of the hemorrhagic class are incorrectly classified as non-hemorrhagic. In comparison, four images of the non-hemorrhagic class are incorrectly classified as hemorrhagic.

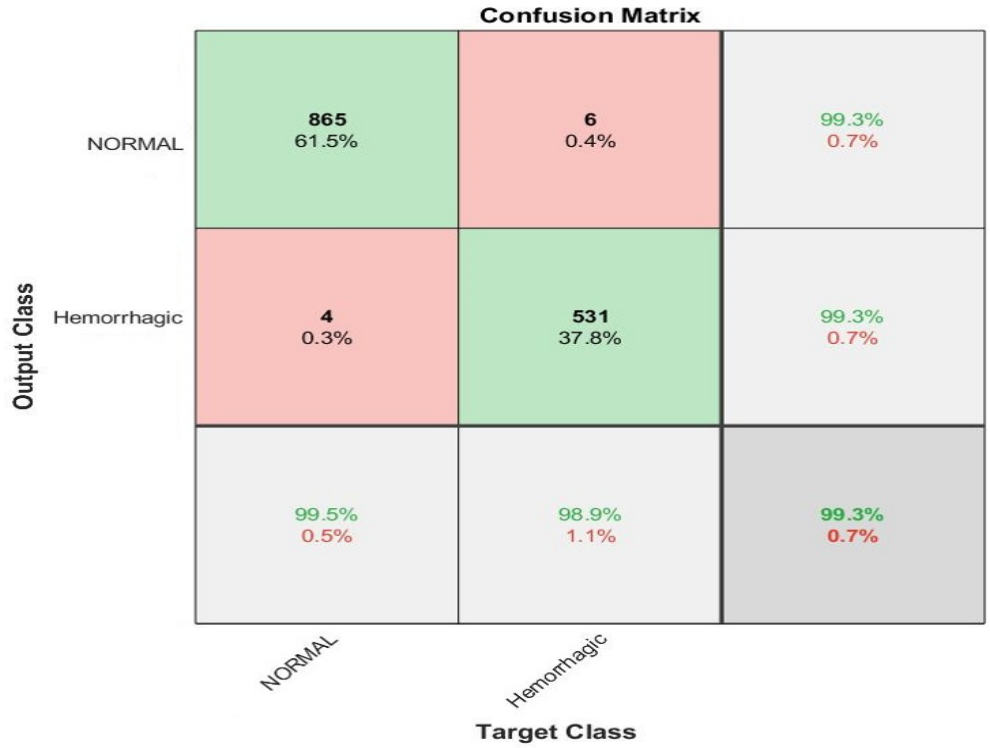

Figure 21. ANN's confusion matrix based on features fused between AlexNet and GLCM and LBP.

Figure 22 shows four slides that were incorrectly classified by the system, where the first row represents two TP slides, meaning that they are non-hemorrhagic slides, but the system classified them as hemorrhagic. Meanwhile, the two slides of the second row represent TN slides, meaning that they are hemorrhagic slides, but the system classified them as non-hemorrhagic.

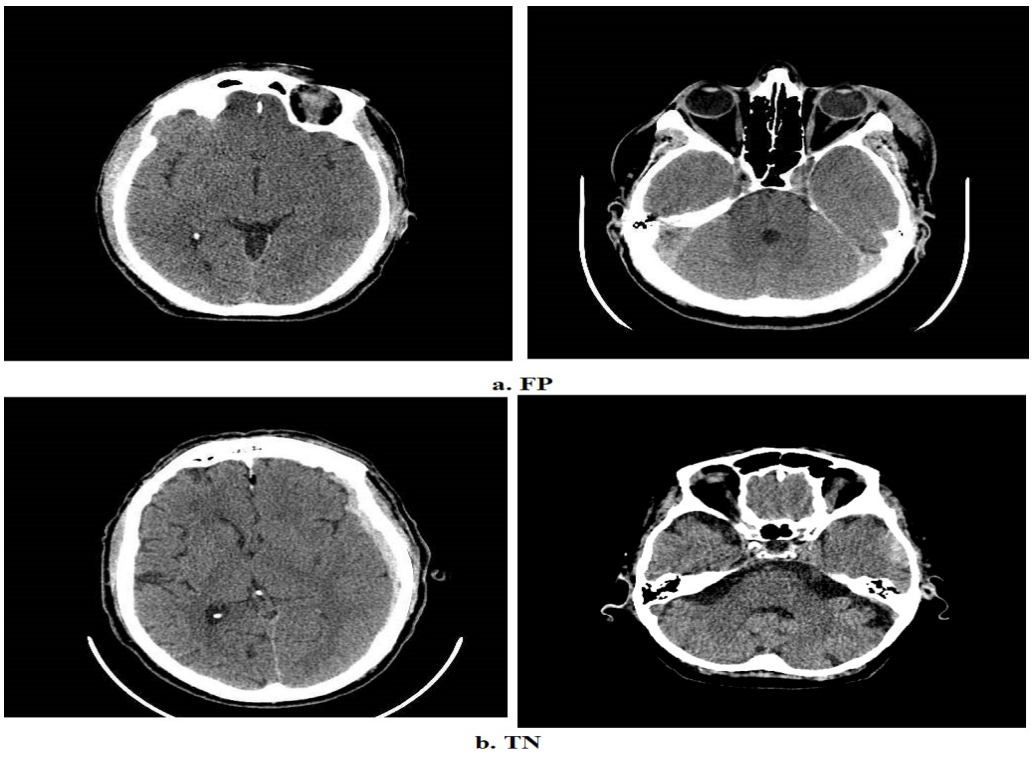

Figure 22. Four samples from the hemorrhagic data set which were incorrectly classified.

5. Discussion and Comparison of the Proposed Methods

ICH and IVH were split at the same time by CT scans using minimally invasive surgery, alteplase and clot lysis [43]. A probabilistic technique based on deep Gaussian processes was developed for training by multi-instance learning and predicting cerebral intracranial hemorrhages. The technique takes the relationships between features using multiple Gaussian layers that outperform single-layer Gaussian operations [44]. Numerous patients with neurological problems received head CT scans. The link between hematoma and clinical factors was demonstrated using a number of univariate and multivariate techniques [45]. The ResNet-18 model was used to discriminate between normal CT and ICH images. In addition to using a Grad-weighted class activation mapping method to detect ResNet-18 decisions [46]. Based on radiology records, a pretrained deep learning network may identify brain haemorrhages. It has been observed that the effectiveness of fine-tuned deep learning models improves the classification results [47]. Using a three-dimensional deep learning network, the subtypes of haemorrhages are segmented in [48]. The CT images were segmented using the area growth method and then optimized.

In this study, three proposed methods have been discussed for evaluating CT images to make a diagnosis for rapid detection of an intracranial hemorrhage. Each proposed system contains more than one model with various methodologies and materials. The study aimed to find an automatic method that helps doctors and radiologists in the rapid diagnosis of an intracranial hemorrhage and determine its location for the patient to receive appropriate treatments. All CT images were improved, all artifacts were removed, and the edges of the hemorrhagic region appeared with the same filters for all the proposed methods. The data augmentation method was used to avoid the overfitting problem during the training phase.

Due to the dataset's limited subject availability and the usage of artificial intelligence techniques in the developed systems, the classification was concentrated at the level of the slide (image) rather than the level of the subject (patient). Additionally, the dataset comprised various numbers of slides for every subject. It is sufficient to diagnose the patient as having hemorrhagic disease if a hemorrhage appears on one of the many patient slides. The dataset was divided into the training, validation and testing stages according to the patient. In contrast to obtaining results at the patient level, results were acquired based on each image, which was more precise. To be more detailed, for the hemorrhagic class, four patients were chosen during the testing phase. Each patient had the following number of slides: 196, 195, 23 and 123. In addition, five patients from the non-hemorrhagic class were chosen. Each patient had 131, 217, 134, 123 and 129 slides. In Figure 21, for instance, we see four images of non-hemorrhagic classes that were incorrectly classified as hemorrhagic and six images of hemorrhagic classes that were wrongly classified as non-hemorrhagic when looking at the confusion matrix. Additionally, due to the small number of images relative to the number of images for each patient, these incorrectly classified images did not accurately represent the patient. Therefore, artificial intelligence systems are classifying images one after the other. As a result, this study diagnosed the CT images of all the proposed systems at the slide level.

The proposed methods in this study are the following. The first proposed method for evaluating CT images to make a diagnosis of the hemorrhagic dataset by CNNs involves pretrained GoogLeNet, ResNet-50 and AlexNet models. The second proposed method is hybrid technology between the CNN models (GoogLeNet, ResNet-50 and AlexNet). The third proposed method is to diagnose the hemorrhagic dataset by an ANN network based on extracting the hybrid features between the CNN models and the GLCM and LBP algorithms and fusing them together.

The first proposed method was the GoogLeNet, ResNet-50 and AlexNet models, where the parameters and training options were tuned to extract deep feature maps and classify them. The GoogLeNet, ResNet-50 and AlexNet models achieved overall accuracies of 94%, 91.7% and 91.5%, respectively. The second proposed method represents a hybrid technique consisting of two blocks: the first block is CNN models to extract the feature maps, and

the second block is the SVM algorithm for classifying the feature maps. The GoogLeNet + SVM, ResNet-50 + SVM and AlexNet + SVM networks achieved overall accuracies of 97.4%, 97.2% and 95.7%, respectively. The third proposed method is to diagnose the hemorrhage dataset with an ANN based on the hybrid features extracted by the GoogLeNet, ResNet-50 and AlexNet models and apply the PCA algorithm to reduce the dimensions of the feature maps and combine them with the hybrid features extracted using the GLCM and LBP algorithms. The ANN network based on combining GoogLeNet feature maps with the features of the GLCM and LBP algorithms achieved 98.9% overall accuracy. When the ANN network was based on the combination of ResNet-50 feature maps with the features of the GLCM and LBP algorithms, the overall accuracy was 99.1%. In comparison, the ANN network reached a 99.3% overall accuracy based on the combination of AlexNet feature maps with the features of the GLCM and LBP algorithms.

Table 7 summarizes the evaluative performance of all proposed methods for CT imaging for the rapid detection of intracranial hemorrhages. First, all the proposed methods reached superior results for the hemorrhage class. The ANN algorithm based on the hybrid features between the CNN models and GLCM and LBP features achieved the best diagnosis of the hemorrhage dataset. It is noted that the best diagnosis of hemorrhage images was accomplished by an ANN classifier based on the features of ResNet-50 + (GLCM and LBP), which reached an accuracy of 99.8%, while the best diagnosis of the hemorrhage images was by the ANN classifier based on the features of GoogLeNet + features (GLCM and LBP), which reached an accuracy of 99.2%.

Table 7. Performance of all proposed methods for CT imaging diagnostics for early detection of hemorrhage disease.

System	Diseases	Hemorrhage	Non-Hemorrhage	Accuracy (%)
Deep Learning	GoogLeNet	92	95.3	94
	ResNet-50	93.1	90.8	91.7
	AlexNet	79.1	99.1	91.5
Hybrid	GoogLeNet + SVM	95.9	98.3	97.4
	ResNet-50 + SVM	96.8	97.4	97.2
	AlexNet + SVM	94.2	96.5	95.7
Hybrid Features ANN	GoogLeNet + (GLCM and LBP)	98.5	99.2	98.9
	ResNet-50 + (GLCM and LBP)	99.8	98.1	99.1
	AlexNet + (GLCM and LBP)	98.9	99.5	99.3

Figure 23 shows the performance of all the proposed methods for CT diagnostics for the fast detection of hemorrhage disease in graph form.

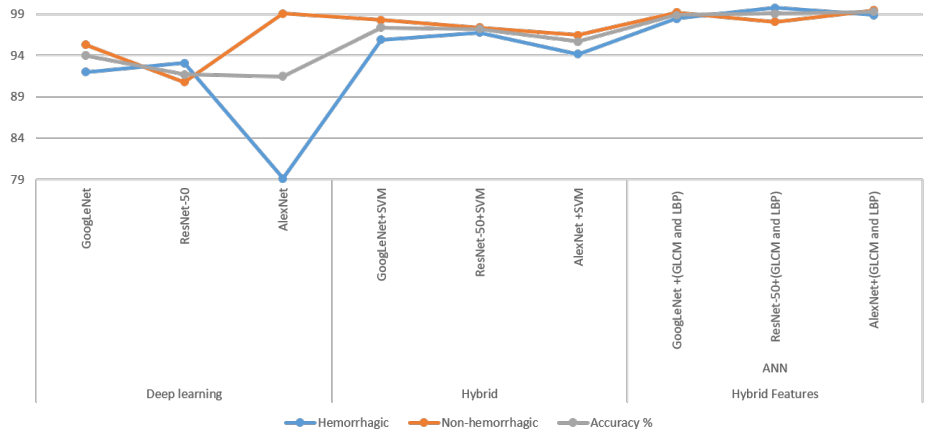

Figure 23. Performance of all proposed methods for fast detection of hemorrhage disease in graph form.

The limitations that we encountered in this study were the small number of patients in the standard dataset, in addition to the dataset not including the characteristics of the patients or the type of cerebral hemorrhage for each patient. Due to the inaccessibility of patients' descriptions, the generalization of our results requires an external validation dataset.

6. Conclusions and Future Works

In this study, the problems of CT image diagnosis for the rapid detection of intracranial hemorrhages were solved by many proposed methodologies, which involve many different methods and materials. All the proposed methods yielded promising results that helped physicians and radiologists make decisions when diagnosing and analyzing hemorrhage images and distinguishing them from suspected images. This paper proposed three methods, each containing more than one system. The first proposed method was to diagnose the hemorrhage dataset using pre-trained CNN models, namely GoogLeNet, ResNet-50 and AlexNet, which achieved accuracies of 94%, 91.7% and 91.5%, respectively. The second proposed method is a hybrid technique between deep learning (GoogLeNet, ResNet-50 and AlexNet) to extract the feature maps and a machine learning algorithm (SVM) to classify the feature maps extracted using deep learning models. GoogLeNet + SVM, ResNet-50 + SVM and AlexNet + SVM achieved superior results, with accuracies of 97.4%, 97.2% and 95.7%, respectively. The third proposed method is to diagnose the hemorrhage dataset using an ANN algorithm based on the hybrid features extracted from the GoogLeNet, ResNet-50 and AlexNet models, reduce the feature dimensions with a PCA algorithm and then combine the features after reducing the dimensions with the features of the GLCM and LBP algorithms. This method obtained the best results compared with the other proposed methods, where the ANN reached an accuracy of 99.3%, precision of 99.36%, sensitivity of 99.5%, specificity of 99.57% and AUC of 99.84% based on the features of AlexNet, GLCM and LBP.

In future works, the proposed systems will be evaluated on a dataset containing cerebral hemorrhage types such as intraventricular, subarachnoid and parenchymal hemorrhages.

Author Contributions: Conceptualization, B.A.M. and Z.G.A.-M.; methodology, E.M.S.; software, B.A.M. and E.M.S.; validation, T.H.R., N.M.M., A.A.S. and A.A.A.; formal analysis, T.S.A.; investigation, F.A.G.; resources, Z.G.A.-M. and B.A.M.; data curation, E.M.S.; writing—original draft preparation, E.M.S.; writing—review and editing, B.A.M. and Z.G.A.-M.; visualization, T.H.R. and N.M.M.; supervision, A.A.A. and A.A.S.; project administration, B.A.M.; funding acquisition, A.A.A. All authors have read and agreed to the published version of the manuscript.

Funding: This research was funded by the Scientific Research Deanship at the University of Ha'il in Saudi Arabia through project number RG-20149.

Data Availability Statement: The data supporting the proposed systems in this study were collected from the hemorrhage dataset available at https://www.kaggle.com/abdulkader90/brain-ct-hemorrhage-dataset (accessed on 10 June 2022).

Acknowledgments: We would like to acknowledge the Scientific Research Deanship at the University of Ha'il in Saudi Arabia for funding this research.

Conflicts of Interest: The authors declare no conflict of interest.

References

1. Balasooriya, U.; Perera, M.U.S. Intelligent brain hemorrhage diagnosis using artificial neural networks. In Proceedings of the 2012 IEEE Business, Engineering & Industrial Applications Colloquium (BEIAC), Kuala Lumpur, Malaysia, 7–8 April 2012; pp. 128–133. [CrossRef]
2. Caceres, J.A.; Goldstein, J.N. Intracranial hemorrhage. *Emerg. Med. Clin.* **2012**, *30*, 771–794. [CrossRef] [PubMed]
3. Badenes, R.; Bilotta, F. Neurocritical care for intracranial haemorrhage: A systematic review of recent studies. *BJA Br. J. Anaesth.* **2015**, *115*, ii68–ii74. [CrossRef]
4. Hemphill, J.C.; Greenberg, S.M.; Anderson, C.S.; Becker, K.; Bendok, B.R.; Cushman, M.; Fung, G.L.; Goldstein, J.N.; Macdonald, R.L.; Mitchell, P.H.; et al. Guidelines for the Management of Spontaneous Intracerebral Hemorrhage. *Stroke* **2015**, *46*, 2032–2060. [CrossRef] [PubMed]

5. Ginat, D.T. Analysis of head CT scans flagged by deep learning software for acute intracranial hemorrhage. *Neuroradiology* **2020**, *62*, 335–340. [CrossRef] [PubMed]
6. Chang, P.; Kuoy, E.; Grinband, J.; Weinberg, B.; Thompson, M.; Homo, R.; Chen, J.; Abcede, H.; Shafie, M.; Sugrue, L.; et al. Hybrid 3D/2D Convolutional Neural Network for Hemorrhage Evaluation on Head CT. *Am. J. Neuroradiol.* **2018**, *39*, 1609–1616. [CrossRef] [PubMed]
7. Karki, M.; Cho, J.; Lee, E.; Hahm, M.H.; Yoon, S.Y.; Kim, M.; Ahn, J.Y.; Son, J.; Park, S.H.; Kim, K.H.; et al. CT window trainable neural network for improving intracranial hemorrhage detection by combining multiple settings. *Artif. Intell. Med.* **2020**, *106*, 101850. [CrossRef] [PubMed]
8. Hee, L.Y.; Seob, C.D.; Wook, R.J.; Jong, Y.J.; Cheol, C.H.; Eun, K.J. Multidetector-Row CT Angiography of Cerebral Vasospasm after Aneurysmal Subarachnoid Hemorrhage: Comparison of Bone Subtraction and Standard CT Angiography with Digital Subtraction Angiography. *J. Korean Soc. Radiol.* **2011**, *65*, 325–331. [CrossRef]
9. Akram, S.U.; Kannala, J.; Eklund, L.; Heikkilä, J. Cell Segmentation Proposal Network for Microscopy Image Analysis. In *Deep Learning and Data Labeling for Medical Applications*; Carneiro, G., Mateus, D., Peter, L., Bradley, A., Tavares, J.M.R.S., Belagiannis, V., Papa, J.P., Nascimento, J.C., Loog, M., Lu, Z., et al., Eds.; Springer International Publishing: Cham, Switzerland, 2016; pp. 21–29.
10. Oyedotun, O.K.; Olaniyi, E.O.; Helwan, A.; Khashman, A. Hybrid auto encoder network for iris nevus diagnosis considering potential malignancy. In Proceedings of the 2015 International Conference on Advances in Biomedical Engineering (ICABME), Beirut, Lebanon, 16–18 September 2015; pp. 274–277. [CrossRef]
11. Helwan, A.; Uzun Ozsahin, D. Sliding window based machine learning system for the left ventricle localization in MR cardiac images. *Appl. Comput. Intell. Soft Comput.* **2017**, *2017*, 3048181. [CrossRef]
12. Simonyan, K.; Zisserman, A. Very Deep Convolutional Networks for Large-Scale Image Recognition. *arXiv* 2014, arXiv:1409.1556.
13. He, K.; Zhang, X.; Ren, S.; Sun, J. Deep Residual Learning for Image Recognition. In Proceedings of the 2016 IEEE Conference on Computer Vision and Pattern Recognition (CVPR), Las Vegas, NV, USA, 27–30 June 2016; pp. 770–778. [CrossRef]
14. Gautam, A.; Raman, B. Towards effective classification of brain hemorrhagic and ischemic stroke using CNN. *Biomed. Signal Process. Control* **2021**, *63*, 102178. [CrossRef]
15. Mohammed, B.A.; Senan, E.M.; Rassem, T.H.; Makbol, N.M.; Alanazi, A.A.; Al-Mekhlafi, Z.G.; Almurayziq, T.S.; Ghaleb, F.A. Multi-Method Analysis of Medical Records and MRI Images for Early Diagnosis of Dementia and Alzheimer's Disease Based on Deep Learning and Hybrid Methods. *Electronics* **2021**, *10*, 2860. [CrossRef]
16. Senan, E.M.; Jadhav, M.E.; Rassem, T.H.; Aljaloud, A.S.; Mohammed, B.A.; Al-Mekhlafi, Z.G. Early Diagnosis of Brain Tumour MRI Images Using Hybrid Techniques between Deep and Machine Learning. *Comput. Math. Methods Med.* **2022**, *2022*, 1–17. [CrossRef]
17. Dawud, A.M.; Yurtkan, K.; Oztoprak, H. Application of deep learning in neuroradiology: Brain haemorrhage classification using transfer learning. *Comput. Intell. Neurosci.* **2019**, *2019*, 4629859. [CrossRef] [PubMed]
18. Tharek, A.; Muda, A.S.; Hudi, A.B.; Hudin, A.B. Intracranial Hemorrhage Detection in CT Scan Using Deep Learning. *Asian J. Med. Technol.* **2022**, *2*, 1–18. [CrossRef]
19. Bobby, J.S.; Annapoorani, C. Analysis of intracranial hemorrhage in CT brain images using machine learning and deep learning algorithm. *Ann. Rom. Soc. Cell Biol.* **2021**, *25*, 13742–13752.
20. Gou, X.; He, X. Deep learning-based detection and diagnosis of subarachnoid hemorrhage. *J. Healthc. Eng.* **2021**, *2021*, 9639419. [CrossRef]
21. Mansour, R.F.; Aljehane, N.O. An optimal segmentation with deep learning based inception network model for intracranial hemorrhage diagnosis. *Neural Comput. Appl.* **2021**, *33*, 13831–13843. [CrossRef]
22. He, J. Automated Detection of Intracranial Hemorrhage on Head Computed Tomography with Deep Learning. In Proceedings of the 2020 10th International Conference on Biomedical Engineering and Technology, Tokyo, Japan, 15–18 September 2020; Association for Computing Machinery: New York, NY, USA, 2020; pp. 117–121. [CrossRef]
23. Chen, R.; Huang, J.; Song, Y.; Li, B.; Wang, J.; Wang, H. Deep learning algorithms for brain disease detection with magnetic induction tomography. *Med. Phys.* **2021**, *48*, 745–759. [CrossRef]
24. Li, L.; Wei, M.; Liu, B.; Atchaneeyasakul, K.; Zhou, F.; Pan, Z.; Kumar, S.A.; Zhang, J.Y.; Pu, Y.; Liebeskind, D.S. Deep learning for hemorrhagic lesion detection and segmentation on brain ct images. *IEEE J. Biomed. Health Inform.* **2020**, *25*, 1646–1659. [CrossRef]
25. Lewick, T.; Kumar, M.; Hong, R.; Wu, W. Intracranial Hemorrhage Detection in CT Scans using Deep Learning. In Proceedings of the 2020 IEEE Sixth International Conference on Big Data Computing Service and Applications (BigDataService), Oxford, UK, 3–6 August 2020; pp. 169–172. [CrossRef]
26. Cortes-Ferre, L.; Gutiérrez-Naranjo, M.A.; Egea-Guerrero, J.J.; Pérez-Sánchez, S.; Balcerzyk, M. Deep Learning Applied to Intracranial Hemorrhage Detection. *Preprints* **2022**, *2021*, 2021120150. [CrossRef]
27. Arab, A.; Chinda, B.; Medvedev, G.; Siu, W.; Guo, H.; Gu, T.; Moreno, S.; Hamarneh, G.; Ester, M.; Song, X. A fast and fully-automated deep-learning approach for accurate hemorrhage segmentation and volume quantification in non-contrast whole-head CT. *Sci. Rep.* **2020**, *10*, 19389. [CrossRef] [PubMed]
28. Lee, J.Y.; Kim, J.S.; Kim, T.Y.; Kim, Y.S. Detection and classification of intracranial haemorrhage on CT images using a novel deep-learning algorithm. *Sci. Rep.* **2020**, *10*, 20546. [CrossRef] [PubMed]
29. Anupama, C.; Sivaram, M.; Lydia, E.L.; Gupta, D.; Shankar, K. Synergic deep learning model–based automated detection and classification of brain intracranial hemorrhage images in wearable networks. *Pers. Ubiquitous Comput.* **2020**, *26*, 1–10. [CrossRef]

30. Cho, J.; Park, K.S.; Karki, M.; Lee, E.; Ko, S.; Kim, J.K.; Lee, D.; Choe, J.; Son, J.; Kim, M. Improving sensitivity on identification and delineation of intracranial hemorrhage lesion using cascaded deep learning models. *J. Digit. Imaging* **2019**, *32*, 450–461. [CrossRef] [PubMed]
31. Helwan, A.; El-Fakhri, G.; Sasani, H.; Uzun Ozsahin, D. Deep networks in identifying CT brain hemorrhage. *J. Intell. Fuzzy Syst.* **2018**, *35*, 2215–2228. [CrossRef]
32. Mansour, R.F.; Escorcia-Gutierrez, J.; Gamarra, M.; Díaz, V.G.; Gupta, D.; Kumar, S. Artificial intelligence with big data analytics-based brain intracranial hemorrhage e-diagnosis using CT images. *Neural Comput. Appl.* **2021**, 1–13. [CrossRef]
33. Abunadi, I.; Senan, E.M. Deep Learning and Machine Learning Techniques of Diagnosis Dermoscopy Images for Early Detection of Skin Diseases. *Electronics* **2021**, *10*, 3158. [CrossRef]
34. Burduja, M.; Ionescu, R.T.; Verga, N. Accurate and efficient intracranial hemorrhage detection and subtype classification in 3D CT scans with convolutional and long short-term memory neural networks. *Sensors* **2020**, *20*, 5611. [CrossRef]
35. Senan, E.M.; Alzahrani, A.; Alzahrani, M.Y.; Alsharif, N.; Aldhyani, T.H. Automated Diagnosis of Chest X-ray for Early Detection of COVID-19 Disease. *Comput. Math. Methods Med.* **2021**, *2021*, 6919483. [CrossRef]
36. Ahmed, I.A.; Senan, E.M.; Rassem, T.H.; Ali, M.A.H.; Shatnawi, H.S.A.; Alwazer, S.M.; Alshahrani, M. Eye Tracking-Based Diagnosis and Early Detection of Autism Spectrum Disorder Using Machine Learning and Deep Learning Techniques. *Electronics* **2022**, *11*, 530. [CrossRef]
37. Kherif, F.; Latypova, A. Chapter 12—Principal component analysis. In *Machine Learning*; Mechelli, A., Vieira, S., Eds.; Academic Press: Cambridge, MA, USA, 2020; pp. 209–225. [CrossRef]
38. Senan, E.M.; Jadhav, M.E. Diagnosis of Dermoscopy Images for the Detection of Skin Lesions Using SVM and KNN. In Proceedings of the the Third International Conference on Sustainable Computing, Jaipur, India, 19–20 March 2021; Springer: Berlin/Heidelberg, Germany, 2022; pp. 125–134.
39. Senan, E.M.; Jadhav, M.E. Techniques for the Detection of Skin Lesions in PH 2 Dermoscopy Images Using Local Binary Pattern (LBP). In Proceedings of the International Conference on Recent Trends in Image Processing and Pattern Recognition, Solapur, India, 21–22 December 2018; Springer: Berlin/Heidelberg, Germany, 2020; pp. 14–25.
40. Senan, E.M.; Abunadi, I.; Jadhav, M.E.; Fati, S.M. Score and Correlation Coefficient-Based Feature Selection for Predicting Heart Failure Diagnosis by Using Machine Learning Algorithms. *Comput. Math. Methods Med.* **2021**, *2021*, 8500314. [CrossRef] [PubMed]
41. Abunadi, I.; Senan, E.M. Multi-Method Diagnosis of Blood Microscopic Sample for Early Detection of Acute Lymphoblastic Leukemia Based on Deep Learning and Hybrid Techniques. *Sensors* **2022**, *22*, 1629. [CrossRef]
42. Al-Mekhlafi, Z.G.; Senan, E.M.; Rassem, T.H.; Mohammed, B.A.; Makbol, N.M.; Alanazi, A.A.; Almurayziq, T.S.; Ghaleb, F.A. Deep Learning and Machine Learning for Early Detection of Stroke and Haemorrhage. *Comput. Mater. Contin.* **2022**, *72*, 775–796. [CrossRef]
43. Sharrock, M.F.; Mould, W.A.; Hildreth, M.; Ryu, E.P.; Walborn, N.; Awad, I.A.; Hanley, D.F.; Muschelli, J. Bayesian deep learning outperforms clinical trial estimators of intracerebral and intraventricular hemorrhage volume. *J. Neuroimaging* **2022**, 1–9. [CrossRef]
44. López-Pérez, M.; Schmidt, A.; Wu, Y.; Molina, R.; Katsaggelos, A.K. Deep Gaussian processes for multiple instance learning: Application to CT intracranial hemorrhage detection. *Comput. Methods Programs Biomed.* **2022**, *219*, 106783. [CrossRef] [PubMed]
45. Tang, Z.; Zhu, Y.; Lu, X.; Wu, D.; Fan, X.; Shen, J.; Xiao, L. Deep Learning-Based Prediction of Hematoma Expansion Using a Single Brain Computed Tomographic Slice in Patients with Spontaneous Intracerebral Hemorrhages. *World Neurosurg.* **2022**, *in press*. [CrossRef]
46. Altuve, M.; Pérez, A. Intracerebral hemorrhage detection on computed tomography images using a residual neural network. *Phys. Med.* **2022**, *99*, 113–119. [CrossRef] [PubMed]
47. Bayrak, G.; Toprak, M.Ş.; Ganiz, M.C.; Kodaz, H.; Koç, U. Deep Learning-Based Brain Hemorrhage Detection in CT Reports. *Stud. Health Technol. Inform.* **2022**, *294*, 866–867.
48. Inkeaw, P.; Angkurawaranon, S.; Khumrin, P.; Inmutto, N.; Traisathit, P.; Chaijaruwanich, J.; Angkurawaranon, C.; Chitapanarux, I. Automatic hemorrhage segmentation on head CT scan for traumatic brain injury using 3D deep learning model. *Comput. Biol. Med.* **2022**, *146*, 105530. [CrossRef]